UNIVERSITÉ DU QUÉBEC À MONTRÉAL

ÉVALUATION DE LA PERFORMANCE ET DE LA SENSIBILITÉ DU MODÈLE RÉGIONAL CANADIEN DU CLIMAT

(MRCC6-GEM5) À SIMULER LA PRÉCIPITATION HORAIRE

MÉMOIRE

PRÉSENTÉ

COMME EXIGENCE PARTIELLE

DE LA MAÎTRISE EN SCIENCES DE L'ATMOSPHÈRE

PAR

KIM LAHAIE

JANVIER 2025

UNIVERSITÉ DU QUÉBEC À MONTRÉAL
Service des bibliothèques

Avertissement

REMERCIEMENTS

Tout d'abord, je souhaite remercier mon directeur de recherche, Alejandro Di Luca, pour son encadrement exceptionnel, ses conseils précieux et sa présence constante tout au long de ce parcours. Son expertise et sa disponibilité ont été essentielles à l'avancement de mes travaux, et je lui suis profondément reconnaissante pour l'apport déterminant qu'il a eu sur ce projet.

Je tiens à remercier les membres du centre ESCER et du Département des sciences l'atmosphère de l'UQAM pour leur appui, en particulier François Roberge, Katja Winger, et Frédérik Toupin, pour leur aide avec les simulations climatiques et les outils informatiques. Je suis également reconnaissante envers le Conseil de recherches en sciences naturelles et en génie du Canada (CRSNG) pour le financement accordé à ce projet.

Je souhaite adresser un grand merci à mes collègues et amis pour leur appui moral et les moments de partage. Tangui a toujours eu des paroles de sagesse à partager, Isabelle s'est distinguée par sa générosité et sa disponibilité, tandis que Margaux, avec son écoute attentive, a souvent trouvé les mots justes pour apaiser mes moments de doute.

Je tiens également à exprimer ma sincère gratitude à Vicente pour sa présence et son soutien durant ces derniers mois. Peu importe ce que l'avenir nous réserve, je resterai toujours reconnaissante pour tout ce qu'il a fait pour moi durant cette étape de ma vie.

Je remercie également ma famille, et tout particulièrement ma maman, même si elle a parfois trouvé que je me compliquais la vie en poursuivant des études supérieures, elle m'a toujours témoigné un amour inconditionnel et un appui constant. Je tiens aussi à exprimer ma profonde gratitude envers mon papa, qui a toujours veillé à m'offrir le meilleur. Son dévouement et sa manière unique de me soutenir, même sans toujours mettre des mots dessus, ont été inestimables et sont toujours restés près de mon cœur.

Enfin, une mention spéciale à Mireille, qui, malgré son caractère grogneur et sa fâcheuse habitude de marcher sur mon clavier, a été une compagne fidèle et constante.

Finalement, je tiens à exprimer ma gratitude à toutes les personnes qui ont contribué, de près ou de loin, à cette réalisation.

TABLE DES MATIÈRES

TABLE DES FIGURES

LISTE DES TABLEAUX

ACRONYMES

AE Absolute Error.

AAE Additive Absolute Error.

CLASS Canadian Land Surface Scheme.

CONUS Contiguous United States.

COSMO COnsortium for Small-scale MOdeling.

CP-RCM Convection-Permitting Regional Climate Model.

CRCM6 Canadian Regional Climate Model (version 6).

ECIF Environmentally Conditioned Intensity-Frequency.

ECMWF European Center for Medium-Range Weather Forecasts.

ESCER Étude et la Simulation du Climat à l'Échelle Régionale.

GEM5 Global Environmental Multiscale model (version 5).

GEM5-12 GEM5 with a 12-km grid spacing.

GEM5-2.5 GEM5 with a 2.5-km grid spacing.

IMERG Integrated Multi-satellitE Retrievals for Global Precipitation Measurement.

ISBA Interaction Soil Biosphere Atmosphere.

LSM Land Surface Model.

MRCC6 Modèle Régional Canadien du Climat (version 6).

NCEP National Centers for Environmental Prediction.

NWS National Weather Service.

P3 Predicted Particle Properties.

RCM Regional Climate Model.

SU Sundqvist.

UQAM Université du Québec à Montréal.

WRF Weather Research and Forecasting.

NOTATIONS

I_ϵ^{AAE} — Intensity component of the absolute additive error.

I^ϵ — Intensity component of the error.

I_n^ϵ — Intensity component of the error normalized by the sum of the total precipitation products.

N — Number of events (per grid point).

N_ϵ^{AAE} — Environment component of the absolute additive error.

N^ϵ — Environment component of the error.

N_n^ϵ — Environment component of the error normalized by the sum of the total precipitation products.

p — Probability of precipitation occurring.

p_ϵ^{AAE} — Frequency component of the absolute additive error.

p^ϵ — Frequency component of the error.

p_n^ϵ — Frequency component of the error normalized by the sum of the total precipitation products.

$P_{x,t}$ — Hourly precipitation field regridded onto the IMERG grid.

PT — Total precipitation.

PT_ϵ^{AAE} — Total precipitation absolute additive error.

PT_ϵ^{AE} — Total precipitation additive error.

R_ϵ^{AAE} — Residual absolute additive error.

t — An hour within the studied period.

W — Vertically integrated water vapor.

x — Each IMERG grid point in the analysis domain.

ω — Vertical velocity in pressure coordinates at 500 hPa.

$\overline{I}^{rain}$ — Average precipitation intensity.

$\widetilde{PT}$ — Total precipitation per grid point.

$\widetilde{PT}^\epsilon$ — Total precipitation per grid point error.

$\widetilde{PT}_n^\epsilon$ — Total precipitation error normalized by the sum of the total precipitation products.

RÉSUMÉ

Les modèles régionaux de climat à convection explicite ont démontré une valeur ajoutée par rapport aux modèles à résolution plus grossière pour la simulation des précipitations, mais l'évaluation de leur précision en fonction de leur résolution et de leur configuration reste un défi. Cette étude évalue la performance et la sensibilité de plusieurs configurations de la sixième version du Modèle Régional Canadien du Climat (MRCC6-GEM5), dans la représentation des précipitations horaires sur le nord-est de l'Amérique du Nord. Plusieurs configurations ont été explorées en variant : l'espacement de la grille horizontale (2,5 km ou 12 km), le paramétrage de la microphysique et la précipitation (Sundqvist ou P3), le modèle de surface terrestre (ISBA ou CLASS), le traitement de la convection profonde (Kain-Fritsch ou explicite), la méthode de pilotage et la version du modèle atmosphérique (GEM5.0.2 ou GEM5.1.1). L'évaluation utilise des jeux de données de précipitation radar et satellite de pointe, y compris les produits Stage IV et IMERG (versions 6 et 7), combinés avec les données de la réanalyse ERA5. Les erreurs de précipitation sont évaluées en utilisant la décomposition intensité-fréquence conditionnée par l'environnement. Cette approche combine des informations sur les erreurs liées aux caractéristiques des précipitations (fréquence et intensité) avec les conditions environnementales associées, incluant les facteurs dynamiques et thermodynamiques. Les résultats montrent que les termes d'erreur influencent collectivement les erreurs totales de précipitation et présentent de fortes compensations, soulignant l'importance de cette méthodologie. La plus grande sensibilité des configurations est observée lors de la modification de la résolution horizontale, la configuration de 2,5 km de grille horizontale améliorant considérablement la simulation des précipitations grâce à des améliorations de la fréquence des précipitations horaires. La version à 2,5 km montre peu de sensibilité aux changements de configurations, même lors de la comparaison de l'impact de la convection profonde paramétrée contre explicite. De plus, de nombreux résultats dépendent de la saison, avec une sensibilité plus élevée durant les mois d'été.

mots clé : précipitations horaires, sensibilité, modèle régionaux à convection explicite

INTRODUCTION

La projection des changements futurs des précipitations – qu'il s'agisse de leur répartition spatiale, de leur chronologie, de leur intensité ou de leur accumulation totale – est cruciale pour anticiper les impacts des changements climatiques. Ces projections précises sont essentielles pour une variété d'applications scientifiques et pratiques, telles que la planification agricole, la gestion durable des ressources en eau, ainsi que la préparation et l'adaptation aux risques climatiques croissants (Trenberth, 2011; Field et al., 2012). Les modèles climatiques globaux sont des outils essentiels pour comprendre les mécanismes climatiques à l'échelle planétaire. Ils permettent de simuler les interactions complexes entre l'atmosphère, les océans et la glace de mer offrant ainsi une vue d'ensemble des changements climatiques potentiels à l'échelle planétaire. En raison de leur résolution spatiale relativement grossière, ils ne sont pas adaptés pour capturer les variations climatiques locales ou régionales. En complément des modèles climatiques globaux, les modèles régionaux de climat permettent d'affiner les projections climatiques en se concentrant sur des régions spécifiques, avec une résolution spatiale plus fine. Cette approche permet de mieux simuler les processus climatiques à l'échelle locale, comme les effets orographiques ou les phénomènes convectifs, qui peuvent avoir un impact significatif sur les conditions climatiques d'une région donnée (Rummukainen, 2010).

Néanmoins, la simulation des précipitations, en particulier à l'échelle horaire, demeure un défi majeur pour les modèles climatiques. Cela est dû à la complexité des processus se produisant à de multiples échelles spatiales et temporelles, allant de la circulation atmosphérique à grande échelle aux interactions microphysiques, dont beaucoup doivent être paramétrés pour être correctement représentés (Tapiador et al., 2019). En effet, la formation des précipitations repose sur deux conditions principales : la présence d'une humidité suffisante dans l'atmosphère et d'un mécanisme permettant la condensation de cette humidité, généralement par un refroidissement de l'air jusqu'à son point de rosée. Ce refroidissement est souvent provoqué par des processus adiabatiques, qui surviennent lorsque l'air est forcé de s'élever, en réponse à des facteurs tels que le soulèvement orographique, le réchauffement de la surface terrestre, les processus convectifs ou encore les fronts météorologiques (Houze Jr, 2014; Trenberth, 2011). Pour simuler les précipitations de manière réaliste, les modèles climatiques doivent représenter adéquatement la variabilité spatio-temporelle de l'humidité atmosphérique, les mécanismes de soulèvement, ainsi que les interactions complexes entre les processus dynamiques et thermodynamiques qui favorisent la condensation. Une représentation imprécise de ces processus, que ce soit en termes de mouvements verticaux de l'air, de distribution de l'humidité ou de profils thermiques, peut conduire à des erreurs substantielles dans les simulations de précipitations

(Tapiador et al., 2019; Randall et al., 2007). Ainsi, une évaluation rigoureuse de la représentation des précipitations horaires dans les modèles climatiques est essentielle. Malgré les défis posés par le manque de données d'observation à haute résolution, il est important d'identifier les limites actuelles des modèles, de comprendre les incertitudes afin d'améliorer la précision des projections climatiques (Tapiador et al., 2019).

La capacité des modèles climatiques à simuler les différentes caractéristiques des précipitations aux échelles sous-journalières et journalières est étroitement liée à leur résolution horizontale (Ban et al., 2014; Di Luca et al., 2016; Knist et al., 2020). L'augmentation de la résolution permet une meilleure représentation des éléments géographiques complexes (tels que les montagnes, les vallées et les lacs) ainsi qu'une amélioration des simulations des précipitations orographiques et convectifs (Ban et al., 2014; Kendon et al., 2012; Leutwyler et al., 2017; Ban et al., 2021; Di Luca et al., 2015; Lucas-Picher et al., 2021; Di Luca et al., 2016). Cependant, il convient de faire preuve de prudence lorsqu'on compare les précipitations simulées par des modèles avec un espacement de grille horizontal d'une dizaine de kilomètres à celles simulées par des modèles avec un espacement de grille horizontal de quelques kilomètres. En effet, il est souvent difficile de déterminer si les différences observées proviennent du changement de résolution horizontale ou de la manière dont les deux versions du modèle traitent les processus convectifs (profonds). Cette ambiguïté découle du fait que la plupart des groupes de recherche désactivent la paramétrisation de la convection profonde lors de simulations utilisant des espacements de grille horizontaux inférieurs à 4 km (e.g. Ban et al., 2014; Kendon et al., 2012; Leutwyler et al., 2017; Berthou et al., 2020). Les modèles régionaux de climat à convection explicite – une sous-catégorie des modèles régionaux généralement caractérisée par des espacements de grilles horizontaux inférieurs à 4 km – s'approchent de l'échelle où la convection profonde peut être explicitement résolue. Cependant, même avec des espacements de grilles inférieurs à 4 km, une grande partie des processus convectifs restent non résolus, car l'échelle des phénomènes convectifs varie considérablement en fonction des conditions météorologiques dominantes, allant de moins de 100 mètres pour la convection peu profonde à quelques dizaines de kilomètres pour les systèmes convectifs organisés (Wyngaard, 2004). Bien que la plupart des chercheurs s'accordent sur cette représentation partielle explicite de la convection pour des espacements de grilles de l'ordre de quelques kilometres, il n'existe pas de consensus général sur la manière spécifique de configurer ces modèles, notamment en ce qui concerne l'inclusion ou non de la paramétrisation de la convection profonde ou de schémas de convection sensibles à l'échelle (Tomassini and Yang, 2022).

De plus, plusieurs processus physiques, qui jouent un rôle crucial dans la formation des précipitations, ne

peuvent pas être directement simulés en raison de la résolution spatiale limitée des modèles. Ces processus doivent donc être paramétrés, ce qui peut introduire des incertitudes dans les simulations. Les schémas de microphysique régissent la formation, la croissance et la combinaison des gouttelettes ou des cristaux de glace de nuage pour produire des précipitations, et influencent des facteurs clés tels que le chauffage diabatique, le refroidissement et la charge en condensats — tous étroitement liés à la flottabilité et à la dynamique des parcelles d'air (e.g. Pruppacher and Klett, 1997). De même, la représentation des processus de surface terrestre peut également jouer un rôle déterminant dans la simulation des précipitations, en influençant les échanges de chaleur et d'humidité entre la surface et l'atmosphère. Par exemple, les variations de l'humidité du sol peuvent affecter de manière significative les précipitations en induisant des changements dans les propriétés de la couche limite (Hohenegger et al., 2009; Schär et al., 1999; Findell and Eltahir, 2003; Liu et al., 2011). Par conséquent, les modèles climatiques peuvent être fortement sensibles aux paramétrisations spécifiques choisies.

Bien que les dynamiques internes d'un modèle régional du climat soient cruciales, elles ne sont pas les seuls déterminants de la performance du modèle dans la simulation des précipitations ; cela dépend également de la qualité des conditions aux frontières qui sont fournies aux limites latérales, (Rummukainen, 2010) et parfois à l'intérieur du domaine (par exemple, par le pilotage spectrale). Les simulations des modèles régionaux peuvent être réalisées selon deux stratégies principales : soit en utilisant aux frontières latérales directement les données de réanalyse pour effectuer la descente d'échelle, soit en adoptant une approche imbriquée avec des résolutions intermédiaires. Ces stratégies peuvent aussi avoir des impacts sur la représentation des précipitations (e.g. Fosser et al., 2020). Pour évaluer les modèles régionaux, ces derniers sont généralement piloté par des réanalyses qui sont souvent considérées comme la meilleure représentation du climat passé récents. Il est important de reconnaître que même les données de réanalyse ne sont pas exemptes d'erreurs, et ces erreurs peuvent se propager dans la simulation du modèle régional (Diaconescu et al., 2007).

Au-delà du fait que la simulation des précipitations dans les modèles climatiques est influencée par de multiples facteurs, plusieurs défis se posent lorsqu'il s'agit d'évaluer la performance et la sensibilité de ces modèles. Comme décrit par Tapiador et al. (2019), les précipitations représentent un « produit final » de la modélisation qui subit l'effet cumulatif des erreurs thermodynamiques et dynamiques. Les métriques d'erreur traditionnelles, telles que le biais ou la racine carrée de l'erreur quadratique moyenne, se limitent à évaluer la précipitation elle-même et peuvent ainsi masquer des erreurs dans les processus physiques

sous-jacents. Pour une évaluation plus complète, il est essentiel d'inclure d'autres variables clés, telles que l'humidité, la température ou le mouvement vertical, afin de mieux comprendre comment le modèle représente les mécanismes menant à la formation des précipitations (Tapiador et al., 2019; Di Luca et al., 2021; Milbrandt et al., 2016). La capacité d'un modèle à reproduire les conditions climatiques passées et présentes ne garantit pas nécessairement sa fiabilité pour les projections futures. En particulier, pour les événements de précipitations extrêmes, les processus physiques sous-jacents peuvent évoluer dans un climat futur, rendant leur simulation plus incertaine (Mikyoung Jun and Nychka, 2008; Mote et al., 2011). Cela souligne l'importance d'élaborer des cadres d'évaluation qui vont au-delà des métriques traditionnelles, en se focalisant sur une analyse détaillée des dynamiques et thermodynamiques impliquées dans la formation et la variabilité des précipitations.

Cette étude vise à évaluer la performance et la sensibilité de la sixième version du Modèle Régional Canadien du Climat (MRCC6-GEM5) dans la simulation des précipitations horaires dans le nord-est de l'Amérique du Nord. Les objectifs principaux sont d'évaluer dans quelle mesure le modèle MRCC6-GEM5 représente les précipitations selon différentes configurations et d'identifier les principales sources d'erreurs. En utilisant la méthode de décomposition de l'intensité-fréquence conditionnée par l'environnement (Di Luca et al., 2021), l'étude vise à quantifier les sources d'erreurs spécifiques et à comprendre les contributions des différents processus physiques à la performance du modèle. L'étude emploie trois jeux de données d'observation à haute résolution parmi les plus avancés : les versions 6 et 7 des Mesures de Précipitations Globales par Satellite Multi-Intégration (IMERG) et le produit de précipitation Stage IV du National Centers for Environmental Prediction. Ces jeux de données fournissent des mesures de précipitations détaillées (horaires, $\Delta x \leq 10$ km) et cohérentes sur le nord-est de l'Amérique du Nord (e.g., Picart et al., 2024), qui sont cruciales pour l'évaluation du modèle. Le produit de réanalyse ERA5 est également utilisé pour évaluer la simulation des conditions environnementales à grande échelle.

Le mémoire est organisé comme suit : le chapitre 1 présente un article scientifique rédigé en anglais, en cours de préparation pour une soumission au Journal of Advances in Modeling Earth Systems. Dans cette article, on y retrouve une description exhaustives des configurations pour les simulations étudiées, un rappel complet de la décomposition de l'intensité-fréquence conditionnée par l'environnement tiré de Di Luca et al. (2021), ainsi qu'une analyse approfondie de la performance des simulations et de leurs principales différences. Le chapitre 1 est suivi d'une conclusion sur l'importance de cette étude et sur l'implication de ce travail. Enfin, trois annexes complètent le document : l'Annexe A présente des comparaisons supplémen-

taires entre les produits d'observation ; l'Annexe B fournit les différences normalisées entre chacune des configurations analysées, et l'Annexe C présente des figures avec des analyses comparables à ce qu'il a été effectué dans l'article, mais avec des simulations différentes.

CHAPITRE 1

EVALUATING THE PERFORMANCE AND THE SENSITIVITY OF THE CANADIAN REGIONAL CLIMATE MODEL AT REPRESENTING HOURLY PRECIPITATION

Ce chapitre est rédigé en anglais et présenté sous la forme d'un article scientifique traitant de l'évaluation de la performance et de la sensibilité du modèle régional canadien du climat (MRCC6-GEM5) dans la simulation des précipitations horaires. François Roberge a contribué à la réalisation de l'ensemble des simulations utilisées dans cette étude. L'article a été rédigé sous la supervision de mon directeur de recherche, le Prof. Alejandro Di Luca, et est en cours de préparation pour une soumission au **Journal of Advances in Modeling Earth Systems** de l'Union américaine de géophysique.

EVALUATION OF THE PERFORMANCE AND SENSITIVITY OF THE CANADIAN REGIONAL CLIMATE MODEL FOR THE REPRESENTATION OF HOURLY PRECIPITATION

Kim Lahaie[1], Alejandro Di Luca[1], François Roberge[1]

[1]*Centre ESCER, Department of Earth and Atmospheric Sciences, Université du Québec à Montréal (UQAM), Montréal, Québec, Canada*

Corresponding author : Kim Lahaie, lahaie.kim@courrier.uqam.ca

ABSTRACT

Convection-permitting regional climate models (CP-RCMs) often outperform coarser-resolution models in simulating precipitation, but assessing their accuracy according to their resolution and configuration remains a challenge. This study evaluates the performance and sensitivity of several configurations of the sixth version of the Canadian Regional Climate Model, based on the fifth version of the Global Environmental Multiscale model (CRCM6-GEM5), in simulating hourly precipitation over northeastern North America. Several configurations are explored by varying : the horizontal grid spacing (2.5 km or 12 km), the schemes related to microphysics and precipitation (Sundqvist or P3), the land surface models (ISBA or CLASS), the treatment of deep convection (Kain-Fritsch or explicit), the driving strategy and the atmospheric model version (GEM5.0.2 or GEM5.1.1). The evaluation uses state-of-the-art radar and satellite precipitation datasets, including Stage IV and IMERG (versions 6 and 7), combined with ERA5 reanalysis data. Precipitation errors are assessed using the Environmentally Conditioned Intensity-Frequency (ECIF) decomposition, which combines information about how precipitation occurs (frequency and intensity) with the environmental (i.e., dynamical and thermodynamical) conditions of its occurrence into three terms. The results show that the three error terms collectively influence the total precipitation errors and exhibit strong compensations, highlighting the importance of this methodology. The greatest sensitivity of the model configuration is observed when modifying the horizontal resolution, with the 2.5-km simulations significantly improving the representation of precipitation compared to 12-km simulations, mainly due to improvements in the hourly frequency of precipitation. The 2.5-km simulations exhibit little sensitivity to changes in configuration, even when activating the Kain-Fritsch scheme to represent the effects of deep convection in simulations. Furthermore, our results vary by season, and the sensitivity of simulations is largest during the summer months.

7

1.1 Introduction

In the context of a changing climate, accurately projecting precipitation, including its location, timing, intensity, and total amount, is critical for a wide range of applications, such as agricultural planning, water resource management, disaster preparedness, and climate adaptation strategies (Field et al., 2012; Trenberth, 2011). Despite its importance, precipitation remains one of the most challenging atmospheric variables to simulate in numerical climate models, largely due to the complex multiscale processes involved (Tapiador et al., 2019). These processes range from large-scale atmospheric circulation to microphysical interactions, many of which must be parameterized due to their occurrence at scales smaller than the model grid (Tapiador et al., 2019; Arakawa and Jung, 2011; Tao and Moncrieff, 2009). Precipitation formation requires both atmospheric moisture and a mechanism to induce condensation, which is often achieved by cooling the air to its dew point. This cooling often results from adiabatic processes as air is forced to rise, driven by mechanisms such as orographic and frontal lift, surface heating and convection (Houze Jr, 2014; Trenberth, 2011). To get precipitation right, climate models must accurately capture the spatial and temporal variability of atmospheric moisture and lifting mechanisms, the feedbacks between dynamical and thermodynamic processes, and the conditions under which condensation occurs. Any errors in the representation of these processes, whether in the representation of vertical air movement, moisture distribution, or temperature profiles-can lead to significant errors in precipitation output (Tapiador et al., 2019; Randall et al., 2007). While the rigorous evaluation of hourly precipitation in climate models is challenging, particularly due to the lack of high-resolution and high-quality observational data, it remains essential for identifying errors, understanding uncertainty, ensuring robustness, and improving the accuracy of climate projections (Tapiador et al., 2019; Kotlarski et al., 2019).

The accuracy of climate models in simulating precipitation on subdaily and daily time scales is tied to their horizontal resolution (Knist et al., 2020; Di Luca et al., 2016; Ban et al., 2014). Compared to Global Climate Models (GCMs), which typically have a horizontal resolution of 50–250 km, Regional Climate Models (RCMs) with resolutions ranging from 10 km down to convection-permitting scales (4 km) provide a significant advantage in capturing finer-scale features. These higher-resolution RCMs are better equipped to represent the intricate details of topographic features such as mountains, valleys, and lakes, which strongly influence local precipitation patterns. This improved spatial resolution enables more realistic simulations of orographic precipitation and localized convective events, which are often inadequately resolved by coarser GCMs (Ban et al., 2021; Lucas-Picher et al., 2021; Leutwyler et al., 2017; Di Luca et al., 2016, 2015;

Ban et al., 2014; Kendon et al., 2012). While these improvements are promising, increasing resolution from 10 km to convection-permitting scales does not uniformly resolve all model biases, significant challenges remain, particularly with respect to persistent biases in model physics and their sensitivity to seasonal variations. To illustrate, Knist et al. (2020) evaluated the performance of the Weather Research and Forecasting (WRF) model in simulating subdaily precipitation patterns over Germany and Switzerland using 12-km and 3-km grid spacings. Knist et al. (2020) showed that while both resolutions exhibit a wet bias due to too frequent light precipitation, this bias is reduced in 3-km runs, the 3-km grid spacing significantly improved the representation (i.e. structure, diurnal cycle and mean precipitation amount) of summer precipitation. Another example is that models with 4 km resolution often improve specific aspects, such as the timing of precipitation within the diurnal cycle compared to models with 10 km resolution, yet they still struggling to accurately capture the amplitude or intensity of these events (Fosser et al., 2015; Prein et al., 2015; Ban et al., 2014; Prein et al., 2013; Kendon et al., 2012).

When comparing simulated precipitation from models with grid spacings of about 10 km and about 3 km, it is often difficult to determine whether the differences are due to the change in horizontal grid spacing or to the specific way in which the two model versions treat (deep) convective processes. This ambiguity arises because most research groups disable the parameterization of deep convection when running simulations with horizontal grid spacings below 4 km (Berthou et al., 2020; Leutwyler et al., 2017; Ban et al., 2014; Kendon et al., 2012). Convection-permitting regional climate models (CP-RCMs) - a subset of RCMs characterized by horizontal grid spacings finer than 4 km - get closer to the scale at which deep convection can be explicitly resolved. However, even at grid spacings below 4 km, some convective processes remain unresolved. The scale of convective phenomena varies significantly depending on the prevailing meteorological conditions, ranging from less than 100 meters for shallow convection to several tens of kilometers for organized convective systems (Wyngaard, 2004). While most researchers agree on the partial explicit representation of convection for grid spacings in the grey zone, there is no general agreement on how to run these models in terms of whether to include the use of parameterizations of deep convection or scale-sensitive convection schemes (Tomassini and Yang, 2022).

Several studies have examined the impact of grid spacing and the representation of deep convection on the accuracy of precipitation simulations, highlighting both improvements and persistent challenges (e.g. Argüeso et al., 2020; Mahoney et al., 2013; Zheng et al., 2016). For instance, Argüeso et al. (2020) compared multiple WRF simulations performed with and without a parameterization of deep convection using

various horizontal grid spacings (32-, 16-, 8-, 4-, and 2-km) to assess the diurnal cycle of precipitation in the Maritime Continent. The timing of the diurnal peak of precipitation of simulations with explicit convection aligned better with the observed timing compared to those using a deep convection scheme. Nevertheless, simulations with explicit convection often exaggerated the amplitude of the diurnal cycle over land, leading to an overestimation of rainfall at the peak hour. Deng and Stauffer (2006) found that simulations with explicit convection at 4-km grid spacing have been shown to misrepresent convective updrafts tied to cold fronts, the convective updrafts were forced on coarser-than-realistic scales, and the rainfall, leading to overly intense rainfall and feedback effects on the atmosphere. High-resolution models that rely solely on cloud microphysics parameterization without incorporating convection schemes may also fail to accurately simulate precipitation and moist convection in specific situations, particularly when small-scale processes dominate (Zheng et al., 2016). A major benefit of CP-RCMs lies in their ability to reduce the excessive buildup of Convective Available Potential Energy (CAPE) and to limit the occurrence of artificial convection, which can appear as grid-scale storms in some simulations (Mahoney et al., 2013).

In addition, the model's simulated precipitation can be highly sensitive to the specific subgrid-scale parameterizations chosen, regardless of how accurately the model's dynamic is simulated (Tapiador et al., 2019). Jankov et al. (2009) performed numerical predictions of five significant precipitation events in California associated with atmospheric rivers during winter using the WRF model with a 3-km grid spacing and four different microphysical parameterizations. The simulations revealed substantial differences in precipitation distribution and cloud structure among the model runs, primarily due to differences in the partitioning of water condensate into different types of hydrometeors among the different microphysical schemes. In their study, Liu et al. (2011) evaluated the sensitivity of cold-season precipitation over Colorado to different model configurations, including seven microphysics schemes and three land surface models (LSMs), using the Advanced Research WRF with a 4-km grid spacing. The microphysics schemes significantly influenced the regional details and showed large differences between the amount of snowfall in valleys and ridges. In contrast, the simulations showed little sensitivity to the choice of LSM used. Music and Caya (2009) conducted four 39-year simulations using the CRCM4 over three basins in North America to assess the sensitivity of water budget components (precipitation, evapotranspiration, vertically integrated atmospheric moisture flux convergence, and runoff) to different LSMs. In the Mississippi and Mackenzie basins, land surface schemes were found to significantly influence water budget components, with precipitation being the exception in the Mississippi basin (Music and Caya, 2009). In the St. Lawrence Basin, precipitation was not affected by changes in LSM (Music and Caya, 2009).

The performance of a RCM in simulating precipitation is not solely determined by the model's intrinsic quality ; it also critically depends on the quality of the driving data provided at the lateral boundaries and sometimes in the interior of the domain (Rummukainen, 2010; Di Luca et al., 2015). The driving data are not error-free, and inaccuracies can propagate into the RCM simulations, potentially impacting precipitation representation (Diaconescu et al., 2007). Furthermore, RCM simulations can be driven using two main strategies : direct downscaling reanalysis data (single nesting approach) or employing a multiple nesting approach with intermediate resolutions. The latter approach mitigates issues related to abrupt resolution jumps, which can exacerbate the spin-up issue (Roberge et al., 2024). For example, Fosser et al. (2020) tested the impact of an intermediate nest within a 4-km resolution model. The study found that when the 4-km model was nested within a 12-km European RCM driven by ERA-Interim, it resulted in significantly different precipitation outcomes compared to single nested approach (directly driven by ERA-Interim). Specifically, the multiple nesting produced more rainfall in both summer and winter due to an increase in frequency, mitigating dry biases seen in the single nesting approach. The study showed that the smoother fields from a direct 80-km (ERA-Interim) to 4-km nesting could impede the spin-up of precipitation events, while the intermediate 12-km nest better supported the development of convection and precipitation within the finer-resolution domain, thus providing an environment that is more conducive to realistic precipitation patterns. However, recent findings suggest that the impact of intermediate simulations can vary based on domain configurations and microphysics parameterizations (Roberge et al., 2024). For instance, while double nesting reduces the required domain size for spin-up and can offer computational advantages, the choice of driving variables (e.g., inclusion of hydrometeors and microphysics schemes) significantly affects the accuracy of precipitation simulations and the extent of spin-up-related artifacts. This highlights the complex interplay between driving data quality, nesting strategy, and model configuration in shaping the performance of high-resolution RCMs.

Beyond the fact that the simulation of precipitation in climate models is influenced by multiple factors, there are several challenges that arise when assessing the performance and sensitivity of these models. As described by Tapiador et al. (2019), precipitation is a 'final' product of modeling that suffers the cumulative effect of errors in both thermodynamics and dynamics. Traditional error metrics (e.g. biais, root mean square) can give an overall impression of good performance that may not reflect the true capabilities of the model (Tapiador et al., 2019; Di Luca et al., 2021; Milbrandt et al., 2016). Moreover, many studies assume that a model will necessarily maintains its reliability for future climate projections. However, research has shown that this assumption may not hold true, particularly for extreme precipitation events, where the phy-

sical processes driving them are likely to shift under future climate conditions (Mikyoung Jun and Nychka, 2008; Mote et al., 2011). This emphasizes the need for evaluation frameworks that extend beyond traditional metrics, focusing instead on a deeper understanding of the underlying dynamics and thermodynamics governing precipitation formation and variability.

This study aims to evaluate the performance and sensitivity of the sixth version of the Canadian Regional Climate Model (CRCM6-GEM5) in representing hourly precipitation in northeastern North America. The main objectives are to assess how well the CRCM6-GEM5 model represents precipitation across different configurations and to identify the primary sources of errors. By using the Environmentally Conditioned Intensity-Frequency (ECIF) decomposition (Di Luca et al., 2021), the study aims to quantify specific error sources and understand the contributions of different physical processes to the overall model performance. The study employs three state-of-art high-resolution observational datasets : versions 6 and 7 of the Integrated Multi-satellitE Retrievals for Global Precipitation Measurement (IMERG) and the National Centers for Environmental Prediction (NCEP) Stage IV precipitation product. These datasets provide detailed (hourly, $\Delta x \leq$ 10 km) and consistent precipitation measurements over northeastern North America (e.g., Picart et al., 2024), which are crucial for model evaluation. The ERA5 reanalysis product is used to provide observed large-scale environmental conditions.

This paper is organized as follows. Section 2 describes the observational and reanalysis data which serve as benchmarks for model evaluation, along with the various configurations of the CRCM6-GEM5 model. Section 3 introduces the ECIF decomposition and the error metrics that are used to quantify model performance. Section 4 presents the results of the model evaluation, highlighting the sensitivity of the model to different configurations. The broader implications of these findings are discussed in Section 5 while Section 6 concludes with a brief summary and an exploration of future research directions.

1.2   Data

1.2.1   Observed and reanalysis data

The evaluation of hourly precipitation is conducted using three high-resolution observational products : two based on satellite data and one based on radar data. These products were selected based on their demonstrated good performance and consistency at representing 3-hourly precipitation data over northeastern North America (Picart et al., 2024).

The first two products correspond to the latest two versions of the Integrated Multi-satellitE Retrievals for Global Precipitation Measurement (IMERG), developed by NASA's Global Precipitation Measurement (GPM) mission. IMERG integrates data from a variety of satellite sensors, including passive sensors (e.g., the Global Precipitation Measurement Microwave Imager (GMI), the Advanced Microwave Scanning Radiometer 2 (AMSR2), and the Special Sensor Microwave Imager/Sounder (SSMIS)) and active sensors (e.g., the Dual-frequency Precipitation Radar (DPR) on the GPM Core Observatory and the CloudSat Cloud Profiling Radar (CPR)). IMERG provides precipitation estimates with global coverage on a regular 0.1° horizontal grid at a 30-minute frequency (Table 1.1). Over land, IMERG data are adjusted using monthly gauge precipitation analyses from the Global Precipitation Climatology Center (GPCC; Huffman et al. (2007)), which account for precipitation undercatch in gauge measurements. The seventh version of IMERG V7, released in July 2023, was used as the main reference product while the previous version, IMERG V6, was used as a complementary comparison product. A brief comparison between both datasets is presented in the *Annexe A*.

The third product is the National Centers for Environmental Prediction (NCEP) Stage IV precipitation product, developed by the National Weather Service (NWS) River Forecast Centers (RFCs; Lin and Mitchell (2005)) hereafter denoted simply as Stage IV. Stage IV is available at an hourly frequency and on a 4-km grid covering the continental United States (CONUS) domain (Prat and Nelson, 2015). Using data from 12 automated hydrometeorological data system gauges, automated surface observation systems, and automated airport weather station reports, the RFC integrates and adjusts estimates for bias in near real time (Prat and Nelson, 2015). This process includes a manual quality control step (Nelson et al., 2016). A comparison with IMERG V7 is available in the *Annexe A*.

The method used to evaluate precipitation requires the use of observed large-scale environmental conditions, which are obtained from the ERA5 reanalysis product. ERA5 is the latest reanalysis from the European Center for Medium-Range Weather Forecasts (ECMWF; Hersbach et al. (2020)). We use the pressure vertical velocity at 500 hPa and vertically integrated water vapor. These variables are available on a regular grid with 0.25° spacing at hourly intervals. The Integrated Forecasting System Cycle 41r2 model generates ERA5 by assimilating observed data from many sources. The reanalysis process incorporates the precipitation rate data from the Stage IV product over the United States.

Table 1.1 Overview of Precipitation Data Sets

Dataset	Description	Reference	ΔX (°)	Int. (h)	Period	Coverage	Source
IMERG	Integrated Multi-satellitE Retrievals for GPM (V6 - V7)	Huffman et al. (2018); Huffman et al. (2020)	0.1	0.5	2000/06 – present	Global	Satellite/gauge
Stage IV	NCEP/EMC US Radar-Est. with Bias Removal	Lin and Mitchell (2005)	~0.05	1	2002/01 – present	CONUS	Surface radar/gauge
ERA5	ECMWF Reanalysis 5 High-Resolution	Hersbach et al. (2020)	0.25	1	2008/01 – present	Global	Reanalysis

1.2.2   CRCM6-GEM5 simulations

This study employs multiple configurations of the sixth version of the Canadian Regional Climate Model (CRCM6-GEM5), currently under development at the ESCER center (*centre pour l'étude et la simulation du climat à l'échelle régionale*) at UQAM (*Université du Québec à Montréal*). The CRCM6-GEM5 model consists of a numerical model that simulates the physical processes in the atmosphere and it is coupled with multiple additional models that simulate processes over different surface types (soil and vegetation, sea ice, glaciers and lakes). The atmospheric processes are based on the fifth version of the Global Environmental Multiscale Model (GEM5; McTaggart-Cowan et al. 2019b; Roberge et al. 2024) that is developed by Environment and Climate Change Canada (ECCC). In this study, GEM5 is coupled with two land surface schemes : the Canadian Land Surface Scheme (CLASS; Verseghy 1991) and the Interaction Soil Biosphere Atmosphere (ISBA; Noilhan and Mahfouf 1996), both of which are described below. Over lakes, GEM5 is coupled with the FLake model (Martynov et al., 2012), while sea ice and glaciers are simulated using single-layer diffusion and force-recovery models (McTaggart-Cowan et al., 2019a).

Several configurations of the CRCM6-GEM5 model are used, including two horizontal grid spacings, two schemes related to microphysics and precipitation, two land surface models, explicit or parameterized deep convection, and two versions of the GEM5 model. Additionally, various driving data strategies are applied. Table 1.2 shows the ten simulations used in this study and Figure 1.1 summarizes the experimental design, highlighting the differences of the configurations. The simulations connected by an arrow indicate that a single change in configuration has been made. The color of the arrows indicates the type of change that was implemented. Further details regarding the various configurations are provided in the following subsections.

Table 1.2 Overview of the CRCM6-GEM5 numerical experiments considered in the study

Simulations name	ΔX (°)	Microphysics scheme	Deep convection	Land surface model	Driving data	GEM5 version
GEM50-12-C-on-SU [ERA5]	0.11°	Sundqvist	Kain-Fritsch	CLASS	ERA5	5.0.2
GEM50-12-C-on-P3 [ERA5]	0.11°	P3	Kain-Fritsch	CLASS	ERA5	5.0.2
GEM50-2.5-C-on-P3 [ERA5]	0.025°	P3	Kain-Fritsch	CLASS	ERA5	5.0.2
GEM50-2.5-C-on-SU [ERA5]	0.025°	Sundqvist	Kain-Fritsch	CLASS	ERA5	5.0.2
GEM50-2.5-I-on-P3 [ERA5]	0.025°	P3	Kain-Fritsch	ISBA	ERA5	5.0.2
GEM50-2.5-I-off-P3 [ERA5]	0.025°	P3	Explicit	ISBA	ERA5	5.0.2
GEM50-2.5-C-off-P3 [ERA5]	0.025°	P3	Explicit	CLASS	ERA5	5.0.2
GEM50-2.5-C-off-P3 [GEM50-12-SU]	0.025°	P3	Explicit	CLASS	GEM5-12	5.0.2
GEM50-2.5-C-off-P3 [GEM50-12-P3]	0.025°	P3	Explicit	CLASS	GEM5-12	5.0.2
GEM51-2.5-C-off-P3 [GEM51-12-P3]	0.025°	P3	Explicit	CLASS	GEM5-12	5.1.1
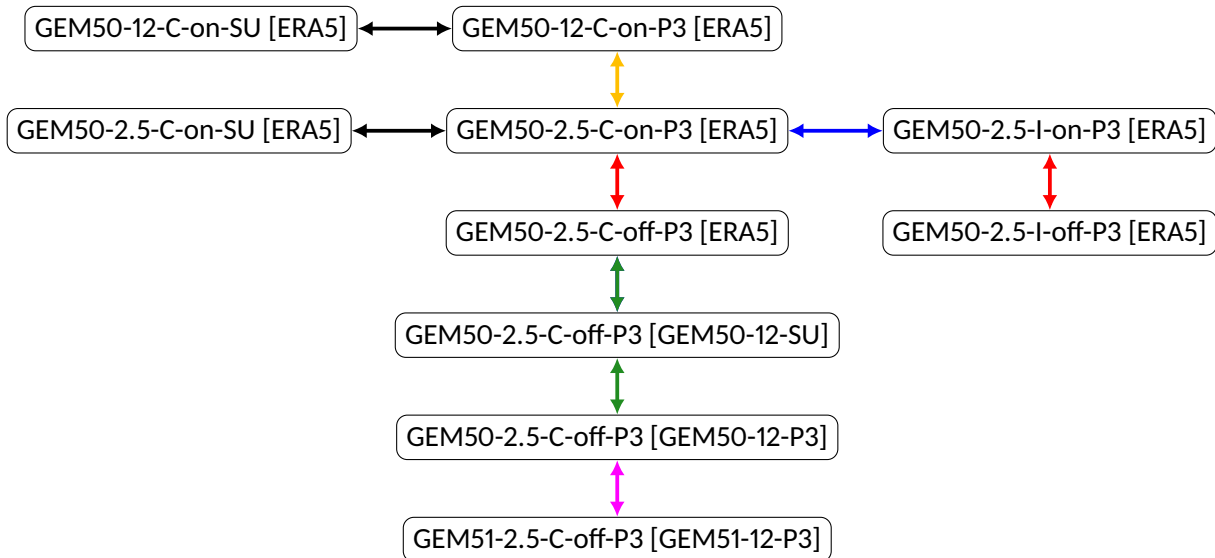
Figure 1.1 Flowchart depicting the configuration differences for the ten simulations used in the study. The naming convention for the simulations is as follows : (GEM5 version) - (grid spacing) - (surface model) - (deep convection)- (microphysics scheme) [driving data]. Arrows represent a single change in configuration : blue for a change in the surface model, red for a change in deep convection, green for a change in the driving data, yellow for a change in the horizontal grid spacing, black for a change in the microphysics scheme, and pink for a change in the GEM5 version. Four different driving data are used : ERA5, GEM50-12-SU, GEM50-P3-12 and GEM51-P3-12.

1.2.2.1 Horizontal grid spacing : GEM5-2.5 and GEM5-12

The CRCM6-GEM5 model is run using two horizontal grid spacings. The lower-resolution simulations have a horizontal grid spacing of 0.11° (approximately 12 km) and are referred to as GEM5-12. All GEM5-12 simulations utilize 71 hybrid vertical levels, with the highest vertical level at 10 hPa, and are run over the Coordinated Regional Climate Downscaling Experiment (CORDEX) North American domain (Giorgi and Gutowski, 2015). This domain encompasses a total of 655 x 655 grid points (excluding grid points in the relaxation or blending zone) and is indicated by the blue line in Figure 1.2. GEM5-12 simulations are driven at the boundaries and in the interior of the domain using data from the ERA5 reanalysis. For the interior of the domain, large-scale spectral nudging is applied to the horizontal wind and temperature variables. This nudging is implemented to atmospheric levels above the 0.85 hybrid level (approximately 850 hPa) and targets horizontal scales larger than 200 km, with a relaxation timescale set to 8 hours (Roberge et al., 2024).

The higher-resolution simulations have a horizontal grid spacing of 0.0225° (approximately 2.5 km) and are referred to as GEM5-2.5. GEM5-2.5 use 66 hybrid levels, distributed in the same manner as in the GEM5-12 version, but with a lower model top at 25 hPa (i.e., it excludes the 5 vertical levels between 25 and 10 hPa). All GEM5-2.5 simulations were run over a domain centered over southern Quebec, Canada, covering a large portion of northeastern North America, with a total of 1330 x 1060 grid points, excluding grid points in the relaxation or blending zone (see the orange line in Figure 1.2). GEM5-2.5 simulations were driven only at the lateral boundaries using either the ERA5 reanalysis or GEM5-12 simulations (see Table 1.2).

1.2.2.2 Condensation and microphysics : Sundqvist and P3

Two schemes are used to represent condensation and precipitation processes : the large-scale condensation scheme of Sundqvist et al. (1989) and the more advanced Predicted Particle Properties (P3) microphysics scheme (Morrison et al., 2015; Milbrandt and Morrison, 2016). The Sundqvist scheme was originally developed for use in global climate models with relatively coarse grid scales, typically in the range of 50 km. Sundqvist uses a single prognostic variable that represents a cloud water/ice category, and the condensation of water vapor occurs when the relative humidity is larger than a predefined value (McTaggart-Cowan et al., 2019a). While this approach is computationally efficient, this scheme does not account for the advection of precipitation, meaning all precipitation falls at the grid point where it forms (Sundqvist et al., 1989).

Figure 1.2 Domains used for the GEM5-2.5 simulations (orange square) and GEM5-12 simulations (blue square). Grid points in the blending or relaxing zones are not included in the displayed domains. Studied domain is colored in green.

The P3 microphysics scheme produces multiple hydrometeors by employing a detailed representation of water vapor, cloud and precipitation microphysical processes. The P3 scheme was developed for finer resolution models, particularly for mesoscale and convective-permitting models with grid scales on the order of 1 to 4 km. The P3 scheme accounts for the formation of cloud droplets through the condensation of water vapor when the air is supersaturated. It simulates the growth of these droplets by vapor condensation. In addition to simple condensation, the P3 scheme also considers the interaction between different hydrometeor types through processes such as coalescence, riming, and aggregation. These processes can lead to the formation of precipitation, which eventually falls out of the cloud when the particles grow large enough. The P3 scheme's ability to handle a broad range of microphysical processes, including the detailed treatment of ice-phase processes, allows it to more accurately simulate mixed-phase clouds and their associated precipitation.

In its current implementation, the P3 scheme adds a total of eight prognostic variables, two for liquid hydrometeors (e.g., liquid cloud mass mixing ratio, q_c, and number mixing ratio, N_c), two for rain hydrometeors (e.g., rain mass mixing ratio, q_r, and number mixing ratio, N_r), and four for ice hydrometeors (e.g., total

ice mass mixing ratio, $q_{i,tot}$, rime mass mixing ratio, $q_{i,rim}$, total ice number mixing ratio, $N_{i,tot}$, and rime volume mixing ratio, $B_{i,rim}$). The increased complexity of P3 compared with Sundqvist implies much more computational resources (Roberge et al., 2024). All simulations using P3 incorporate a subgrid cloud and precipitation fraction (SCPF) scheme (Chosson et al., 2014; Jouan et al., 2020).

1.2.2.3   Deep convection scheme : explicit and parametrized

In Table 1.2, simulations with the deep convection scheme activated are labeled as 'on,' while those without it are labeled as 'off'. The Kain-Fritsch deep convection scheme (Kain and Fritsch, 1990; McTaggart-Cowan et al., 2019b) is a mass flux scheme that triggers deep convection based on the temperature and humidity profile, and the grid-scale vertical velocity. If triggered, the scheme produces clouds and precipitation, and releases latent heat. The scheme redistributes heat and moisture vertically and considers detrainment and entrainment processes. The closure occurs when 90% of the initial Convective Available Potential Energy (CAPE) is eliminated from the environment. GEM5-2.5 simulations were conducted with explicit deep convection and with Kain-Fritsch deep convection scheme. It is important to note that GEM5-2.5 simulations employ a partially explicit treatment of convection, the Kuo Transient shallow convection scheme (Bélair et al., 2005) is used and can produce precipitation. All GEM5-12 simulations were performed using the Kain-Fritsch deep convection scheme, GEM5-12 simulations use the shallow convection scheme of Bechtold et al. (2001), which does not produce precipitation.

1.2.2.4   GEM5 model version : GEM 5.0.2 and GEM 5.1.1

Two GEM5 model versions are used : version 5.0.2 (denoted as GEM50) and version 5.1.1 (denoted as GEM51). Both versions include multiple updates across different components of the model, including changes in the surface layer scheme, the land surface scheme, and the microphysics scheme. To maintain land-atmosphere coupling under very stable conditions, the GEM50 model imposes a minimum wind-speed threshold at the lowest level. In contrast, to deal with very stable regimes, the GEM51 model uses a minimum Obukhov length of 20 m that also ensures a minimum level of turbulence (McTaggart-Cowan et al., 2019b; Whittaker et al., 2024). There are also updates in the land model. In GEM50, the depth of the bedrock is capped at 3 meters and is based on root depth. In contrast, GEM51 determines bedrock depth from the depth of geophysical input data. Additionally, the version 3.6 of the CLASS land surface scheme used in GEM51 includes a correction for water vapor flux, improving the calculation of evaporation. Finally, GEM51 includes several bug fixes compared to GEM50, regarding the P3 microphysics scheme. While these up-

dates have shown to affect the simulation of cloud and precipitation processes, the degree and the specific contributions of each change remain uncertain. Further sensitivity analyses are required to disentangle and quantify their individual impacts.

1.2.2.5   Land surface model : ISBA and CLASS

Land surface model can influence precipitation through various mechanisms, such as altering water vapor availability via evapotranspiration and modulating the initiation of convection through surface moisture and temperature fluxes. Two different LSMs are employed : ISBA and CLASS. ISBA (Bélair et al., 2003) focuses on a simplified representation of the exchanges between the land surface and the atmosphere. ISBA models the transfer of water and energy between the soil, vegetation, and atmosphere by relying on these parameterized processes, which include key factors like soil moisture availability, leaf area index, and root depth.

CLASS (Verseghy, 1991) uses a more detailed treatment of soil layers, vegetation types, and snow processes than ISBA. In CLASS, evaporation is modeled as part of the broader process of evapotranspiration, which includes both the direct evaporation of water from the soil and the transpiration of water through plants. The model simulates the vertical movement of water within the soil, accounting for processes like infiltration and percolation, which influence how much water is available for evaporation. The model also integrates vegetation processes by simulating how plants take up water from the soil and release it into the atmosphere through transpiration.

1.2.2.6   GEM5-2.5 driving strategies : single and double nesting

All GEM5-12 simulations and some GEM5-2.5 simulations are driven directly by the ERA5 reanalysis, and are indicated by [ERA5] in their names (see Table 1.2 and Figure 1.1). Simulations are driven at the lateral boundaries using horizontal wind components, temperature, geopotential height and specific humidity from 37 pressure levels. In addition, GEM5-12 simulations are also driven in the interior of the domain using large-scale spectral nudging as explained in Section 1.2.2.1

Additionally, some GEM5-2.5 simulations use a double-nesting approach, where an intermediate GEM5-12 simulation serves as a bridge between the coarser driving data (i.e., the ERA5 reanalysis) and the finer-scale GEM5-2.5 simulation. For example, GEM5-2.5-C-off-P3 [GEM50-12-SU] is driven by output from a GEM5-12

simulation that employs the Sundqvist scheme. In this double-nesting configuration, GEM5-2.5 is driven at the lateral boundaries using horizontal wind components, temperature, and specific humidity on 71 model levels, along with surface orography (geopotential height) and all eight 3D prognostic variables from the P3 microphysics scheme.

1.3 Methodology

1.3.1 Regridding observed and simulated data

Given that specific attributes of precipitation are strongly dependent on the spatial and temporal resolution of the data, one of the first challenges is the direct comparison of precipitation rates derived from datasets with different temporal and/or spatial resolutions. As noted in Lucas-Picher et al. (2017), one approach is to present the observational and model datasets in their native grid formats to preserve the spatial nuances that can add value. However, this can lead to discrepancies due to differences in resolution; finer-resolution datasets (such as the 2.5 km simulations in our study) may exhibit more extreme values compared to coarser-resolution datasets (like the 12 km simulations in our study). An alternative approach is to aggregate the observed and simulated datasets onto a common grid, typically the coarsest grid, to address the resolution mismatch. This method reduces discrepancies arising from different resolutions but may result in the loss of finer-scale information and the added value it provides (Di Luca et al., 2021; Lucas-Picher et al., 2017). Considering these trade-offs, we opted to regrid all datasets onto the IMERG grid at 0.1° using conservative interpolation from the *xESMF* Python library (`https://xesmf.readthedocs.io/en/stable/index.html`).

The study focuses on northeastern North America (Figure 1.2), excluding the Canadian region, as Stage IV data is limited to the United States. In addition, the IMERG V6 product has been found to produce less reliable results over Canada during winter, as documented in Picart et al. (2024). To address the spatial spin-up issue, grid points within 15 grid cells (approximately 150 km) from the boundaries of which the simulations were conducted were excluded from the analysis, following the findings of Roberge et al. (2024). After these adjustments, the analysis domain consists of a total of 12,960 IMERG grid points (Figure 1.2). Hourly mean precipitation values from all datasets were compared over a two-year period, from January 2016 to December 2017, which represents the longest period common to all available simulations. Additional results evaluated over a four-year period were consistent with those of the two-year period (not shown).

For each dataset, the hourly precipitation field regridded onto the IMERG grid is denoted as $P_{x,t}$, where x represents each IMERG grid point in the analysis domain and t represents an hour within the study period. Each precipitation value, denoted as $P_{x,t}$, has a corresponding vertical pressure velocity at 500 hPa, represented by the variable $\omega_{x,t}$, and a vertically integrated water vapor value, represented by the variable $W_{x,t}$. The simulations compute precipitation, vertical velocity, and integrated water vapor, while there are no direct observations of these two latter variables. Consequently, the values of ω and W are derived from the ERA5 reanalysis for the observational data set. To focus on large-scale dynamical features of ω, a Gaussian filter with a standard deviation of 3 (corresponding to a kernel radius of $\sim$ 120 km) was applied using *scipy.ndimage.gaussian_filter* in Python. It should be noted that while Gaussian filtering smooths the field, it impacts all scales of the variable and does not exclusively preserve large-scale behaviors. Instead, it attenuates smaller-scale variability more strongly, which emphasizes larger-scale patterns in the resulting field.

1.3.2   Precipitation decomposition and error metrics

In this study, we use the "Environmentally Conditioned Intensity-Frequency (ECIF) decomposition," a methodology developed by Di Luca et al. (2021). This approach combines two independent decompositions. The initial decomposition consists of dividing the precipitation into discrete dynamic and thermodynamic regimes, based respectively on vertical pressure velocity at 500 hPa and column-integrated water vapor. The second decomposition consists of dividing precipitation into three terms representing distinct aspects of the precipitation process : large-scale environmental conditions, frequency, and intensity of hourly precipitation.

The first decomposition involves binning $\omega_{x,t}$ (vertical pressure velocity at 500 hPa) and $W_{x,t}$ (vertically integrated water vapor) into distinct categories, with $\omega_{x,t}$ falling within the interval $[\omega_i, \omega_{i+1}]$ and $W_{x,t}$ within $[W_j, W_{j+1}]$. Each combination of intervals (i,j) is referred to as a "regime." Precipitation rates $(P_{x,t})$ at a given grid point x and time t are remapped into the corresponding regime space based on their associated values of $\omega_{x,t}$ and $W_{x,t}$, such that $P_{x,t} \longrightarrow P_{i,j,n_{i,j}}$. This decomposition enables an evaluation of the dependence of precipitation on environmental conditions, specifically dynamical conditions ($\omega_{x,t}$) and thermodynamic conditions ($W_{x,t}$).

Within each regime (i,j), there are a total number of hours $N_{i,j}$, indexed by $n_{i,j}$, where $n_{i,j}$ ranges from 1 to $N_{i,j}$. The index $n_{i,j}$ uniquely identifies each hour that satisfies the conditions of regime (i,j), allowing for systematic analysis of precipitation rates. For these hours, the mean precipitation intensity is denoted

as $\overline{I}_{i,j}$. Consequently, the total precipitation in regime (i, j), $PT_{i,j}$, can be expressed as :

$$PT_{i,j} = \sum_{n_{i,j}=1}^{N_{i,j}} P_{i,j,n_{i,j}} = N_{i,j} \cdot \overline{I}_{i,j} \tag{1.1}$$

To start the second decomposition, it is necessary to define hourly precipitation events. These are defined as hours where the total hourly precipitation exceeds a threshold of 1/24 mm h^{-1}, following Di Luca et al. (2021). The precipitation events within a regime (i, j) are characterized by their number and intensity, denoted as $N_{i,j}^{rain}$ and $\overline{I}_{i,j}^{rain}$, respectively. Unlike $N_{i,j}$, which accounts for all hours in a regime, $N_{i,j}^{rain}$ considers only those hours classified as precipitation events. Similarly, $\overline{I}_{i,j}^{rain}$ represents the mean precipitation intensity during these events, as opposed to $\overline{I}_{i,j}$, which averages intensity across all hours in the regime. Using these event-specific quantities, the total precipitation in each regime can be approximated as :

$$PT_{i,j} \approx N_{i,j}^{rain} \cdot \overline{I}_{i,j}^{rain}. \tag{1.2}$$

The number of precipitation events in each regime, $N_{i,j}^{rain}$, can be expressed as the product of the total number of hours in the regime, $N_{i,j}$, and the probability of precipitation occurring under the specific environmental conditions of that regime, $p_{i,j} = \text{prob}(\text{rain} \mid (\omega_i, W_j))$. Using this relationship, the total precipitation in the regime can be approximated as :

$$PT_{i,j} \approx N_{i,j} \cdot p_{i,j} \cdot \overline{I}_{i,j}^{rain} \tag{1.3}$$

In summary, the second decomposition expresses total precipitation in three different components. The first component reflects the number of times the model simulates certain environmental conditions, regardless of whether precipitation occurs. The second component represents the probability of precipitation occurring under those conditions. The third component quantifies the intensity of precipitation conditional on its occurrence.

The total precipitation in each regime ($PT_{i,j}$) depends on the size of the domain (i.e. the number of grid points) and the duration of the analysis period. To ensure comparability across regions of varying sizes, the total precipitation is normalized ($\widetilde{PT_{i,j}}$) to represent the precipitation per grid point. Similarly, $N_{i,j}$ is normalized to indicate the average number of hours per grid point within a given regime. This normalization allows for a consistent interpretation of precipitation metrics, independent of the spatial extent of the domain.

The normalized version of Equation 1.3 is used to represent the modeled (m) and the observed (o) total precipitation to calculate the simulated total precipitation error in each regime :

$$
\begin{aligned}
\widetilde{PT}^{\epsilon} &= \widetilde{PT}^{m} - \widetilde{PT}^{o} \\
&= N^m \cdot p^m \cdot \overline{I}^{rain,m} - N^o \cdot p^o \cdot \overline{I}^{rain,o} \\
&= \Delta N \cdot p^o \cdot \overline{I}^{rain,o} + \Delta p \cdot \overline{I}^{rain,o} \cdot N^o + \Delta \overline{I}^{rain} \cdot N^o \cdot p^o + R^{\epsilon} \\
&= N^{\epsilon} + p^{\epsilon} + I^{\epsilon} + R^{\epsilon}
\end{aligned}
\tag{1.4}
$$

where Δ represents the difference between modeled and observed values (e.g., $\Delta N = N_m - N_o$). Equation 1.4 clearly indicates that errors in the total precipitation for each regime (i, j) can be attributed to four distinct components :

1. N^{ϵ} is related to the ability of the model to simulate the observed frequency of specific large-scale environmental conditions ("regimes"). This error component is zero only if the model accurately simulates the observed frequency of occurrence ($N^m = N^o$). This error is referred to as the "environment" component of the error.

2. p^{ϵ} is related to the ability of the model to simulate the observed number of precipitation events under certain environmental conditions. If the simulated probability of precipitation is equal to the observed probability ($p^m = p^o$), this error component is zero. This error is referred to as the "frequency" component of the error.

3. I^{ϵ} is related to the ability of the model to produce the correct precipitation rate under the given environmental conditions. If the simulated precipitation intensity matches the observed intensity ($I^{rain,m} = I^{rain,o}$), this error component is zero. This error is referred to as the "intensity" component of the error.

4. R^{ϵ} is related to interaction terms and is referred to as the "residual" component of the error. This component is expected to be small compared to the other error components and can be defined as

$$
R^{\epsilon} = \Delta N \cdot \Delta p \cdot \overline{I}^{rain,o} + \Delta p \cdot \Delta \overline{I}^{rain} \cdot N^o + \Delta \overline{I}^{rain} \cdot \Delta N \cdot p^o + \Delta p \cdot \Delta \overline{I}^{rain} \cdot \Delta N
\tag{1.5}
$$

When neither the simulations nor the observations in any particular regime reveal any precipitating events, the computation of the error using Equation 1.4 is clearly defined. Equation 1.4 cannot determine the error in a regime where only one of the two data sets exhibits certain precipitating events. In this scenario, the error is defined as the value of the missing precipitation in either data set, with a minus sign for missing precipitation in the model and a plus sign for missing precipitation in the observations. In these situations,

we presume that the error is associated to the large-scale environmental component of the error and the frequency and intensity are defined as null. Additionally, to ensure robustness, only regimes with at least five precipitating events in either the observations or the model are included in the analysis.

From Equation 1.4, it becomes apparent that within a specific regime, a zero total precipitation error can be obtained by balancing positive and negative errors across various error components. Similarly, it is also possible to compensate errors across different regimes. To evaluate the degree to which a simulation produces a small total precipitation error by compensating errors between individual error terms, we use two error metrics that were introduced by Di Luca et al. (2021). The first error metric is the absolute error (AE) and allows for all error compensations (including those across different regimes and error terms) :

$$PT_\varepsilon^{AE} = \left| \sum_{i,j} \widetilde{PT}_{i,j}^\epsilon \right| = \left| \sum_{i,j} \left(N_{i,j}^\epsilon + p_{i,j}^\epsilon + I_{i,j}^\epsilon + R_{i,j}^\epsilon \right) \right| \tag{1.6}$$

The second error metric is referred to as the additive absolute error (AAE) and prevents any error compensations. It is calculated by summing the absolute error of all individual regime and error terms :

$$PT_\epsilon^{AAE} = \sum_{i,j} \left| N_{i,j}^\epsilon \right| + \sum_{i,j} \left| p_{i,j}^\epsilon \right| + \sum_{i,j} \left| I_{i,j}^\epsilon \right| + \sum_{i,j} \left| R_{i,j}^\epsilon \right| \tag{1.7}$$

To assess the individual contributions of each errors terms, we also define :

$$N_\epsilon^{AAE} = \sum_{i,j} \left| N_{i,j}^\epsilon \right| \tag{1.8}$$

$$p_\epsilon^{AAE} = \sum_{i,j} \left| p_{i,j}^\epsilon \right| \tag{1.9}$$

$$I_\epsilon^{AAE} = \sum_{i,j} \left| I_{i,j}^\epsilon \right| \tag{1.10}$$

$$R_\epsilon^{AAE} = \sum_{i,j} \left| R_{i,j}^\epsilon \right| \tag{1.11}$$

1.4   Results

1.4.1   Observed decomposed precipitation

Figure 1.3 presents the application of the ECIF decomposition to the IMERG V7 hourly data over the continental northeastern North America domain (12 960 IMERG grid points ; Figure 1.2) which includes two years

of data (17 544 hours), totaling more than 2.27×10^8 hourly values. As indicated in Equation 1.3, the cumulative precipitation per grid point (Figure 1.3a) is obtained by multiplying three factors : the number of events per grid point within each regime (Figure 1.3b), the probability of events precipitating (Figure 1.3c), and the average intensity of the precipitating events (Figure 1.3d).
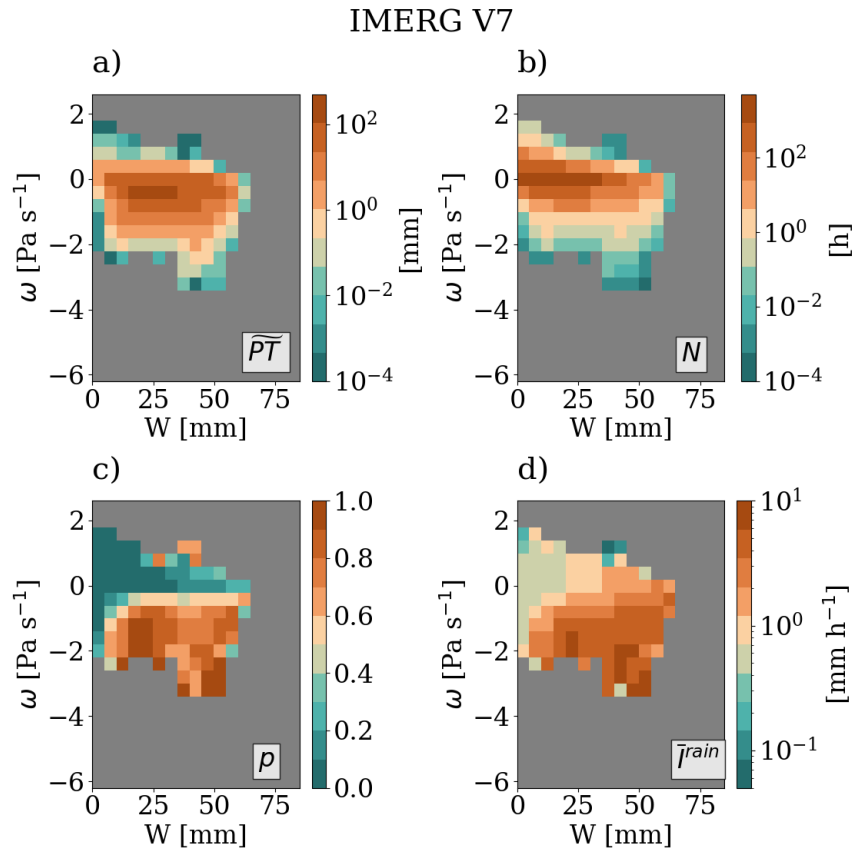
Figure 1.3 Application of the ECIF method on IMERG V7 precipitation datasets from January 2016 to December 2017. The subplots display : (a) total precipitation per grid point, (b) the number of occurrences of environmental conditions per grid point for each regime, (c) the probability of precipitation occurrence within each regime, and (d) the intensity of precipitation in each regime. The regimes are defined based on the vertically integrated water vapor in the column (W), binned from 0 to 80 mm in 5 mm increments, and the pressure velocity at 500 hPa (ω), binned from -6.2 to 2.2 Pa s^{-1} in 0.4 Pa s^{-1} increments. Both variables are derived from the ERA5 reanalysis data.

Figure 1.3a shows that the total precipitation per grid point peaks at over 100 mm of rain for regimes with slightly negative vertical pressure velocity (ω between -0.2 and -0.6 Pa s^{-1}) and moderate water vapor values (W between 20 and 40 mm). The decomposition terms (Figures 1.3b-d) show that total precipitation is influenced by different factors depending on the regime. For example, in regimes with strong dynamical forcing ($\omega \leq$ -1 Pa s^{-1}), total precipitation is primarily driven by high probability and intensity. This means that although these regimes are relatively infrequent, they produce precipitation frequently, and when it

does occur, it tends to be intense, contributing significantly to total precipitation. In contrast, the regimes having the highest total precipitation values are dominated by environmental conditions. This suggests that the main contribution to the total precipitation comes from the high frequency of regimes characterized by slightly negative vertical pressure velocity and moderate water vapor values, rather than from the intensity or frequency of individual events. The number of events (N) shows that the highest values reach up to 2000 events per grid point for near-zero vertical pressure velocity (ω between 0.2 and -0.2 Pa s^{-1}) and W less than 40 mm. The number of events per regime is highly sensitive to changes in ω values, while showing relatively weak sensitivity to changes in W (Figure 1.3b). Figure 1.3c shows that the probability of precipitation occurrence (p) is below 0.1 for regimes with positive or near-zero vertical velocities and low humidity environments and increases strongly with stronger ascending motion and higher integrated water vapor. For regimes with $\omega \leq$ -0.6 Pa s^{-1} and $W \geq$ 15 mm, the probability of precipitation is generally greater than 70%. Similarly, the mean intensity of precipitation ($\overline{I}^{rain}$) increases with both W and more negative ω values, peaking at about 10 mm h^{-1} under strong ascending motion and high water vapor values (Figure 1.3d). Finally, Figures 1.3a–d illustrate that the strongest ascending motions occur exclusively with relatively high values of W, resulting in a slightly elongated pattern in the occurrence of regimes.

Figure A.1 in the *Annexe A* shows the comparison between IMERG V6 and IMERG V7 using the ECIF error decomposition. This figure indicates that there is substantial compensation between the intensity and frequency of precipitation between both versions. For instance, IMERG V6 produces higher probability of precipitation while displaying lower precipitation intensity compared to IMERG V7. Figure A.2 in the *Annexe A* shows the comparison between Stage IV and IMERG V7 and also indicates that there is substantial compensation between the intensity and frequency of precipitation. Figure A.2 additionally shows that the mean intensity of precipitation in Stage IV exhibits a more pronounced sensitivity to W values than IMERG V7, with lower intensities for low W and higher intensities for moderate and high W values. As it will be shown in more detail in Section 1.4.4, the differences among the various observational datasets are generally much smaller than those between the simulations and the observations. Overall, the results are largely robust to the choice of observational data.

1.4.2   GEM5-12 precipitation errors decomposition

Figure 1.4 shows the errors in the GEM50-12-C-on-SU [ERA5] simulation evaluated against the IMERG V7 dataset using the ECIF error decomposition. As indicated in Equation 1.4 the total precipitation error per

grid point (Figure 1.4a) can be expressed as the sum of four errors terms : the environment error (Figure 1.4b), the frequency error (Figure 1.4c), the intensity error (Figure 1.4d) and the residual error (not shown). The markers denote the regimes where there is consistency in the error sign between the simulation and the IMERG V6, IMERG V7, and Stage IV observed datasets. Regimes depicted in white in Figure 1.4c-d are defined as null, as defined in the methodology (see Section1.3.2).

Figure 1.4 GEM50-12-C-on-SU [ERA5] error against IMERG V7 for the total precipitation per grid point (a) and the three decomposition terms : environment error (b), frequency error (c), and intensity error (d). The white regimes represent errors that are defined as null (see Section1.3.2). The markers in panels a, c and d indicate the regimes where there is an agreement in the sign of the error using IMERG V6, IMERG V7 and Stage IV. Only regimes with at least five precipitating events are considered in this analysis.

Figure 1.4a shows that the total precipitation is generally overestimated across most regimes, except for those where $\omega \geq$ -0.6 Pa s^{-1} and $W \geq$ 25 mm, and there is a general agreement in the error sign when considering all three observational datasets. The environment error (Figure 1.4b) exhibits a mix of underestimations and overestimations depending on the regime considered. Figure 1.4c shows a systematic overestimation of the frequency error terms relative to all three observational products (IMERG V6, IMERG V7, Stage IV), indicating that GEM50-12-C-on-SU [ERA5] triggers precipitation too frequently across all regimes.

Figure 1.4d shows that the intensity of precipitation is largely underestimated by the simulation of GEM50-12-C-on-SU [ERA5] relatively to all observational products, for regimes with $\omega \geq$ -0.6 Pa s^{-1}, suggesting that the excess of precipitation frequency is somewhat compensated by a lower intensity. For regimes with $\omega \leq$ -1 Pa s^{-1} and $W \geq$ 30 mm, the simulation of GEM50-12-C-on-SU [ERA5] shows a positive bias, indicating a stronger intensity relative to all observations. As these regimes are often associated with the highest precipitation rates (see Figure 1.3), this error suggests that the simulation overestimates hourly precipitation extremes. For all error terms (Figure 1.4a-c-d), the sign of the error appears to be robust to the choice of the observational product, suggesting that errors are outside the observational uncertainty. In *Annexe B*, the normalized errors are calculated by dividing the error by the sum of the precipitation values from the two compared products. Figure B.1 illustrates that frequency and intensity are the primary contributors to the overall errors. Frequency contributes significantly to the errors in regimes characterized by low water vapor or ascending vertical velocity, while intensity plays a major role in regimes associated with more extreme precipitation.

Figure 1.5 shows the difference between the ECIF decomposition terms for the 12-km simulation using the P3 microphysics scheme (GEM50-12-C-on-P3 [ERA5]) and the one using the Sundqvist condensation scheme (GEM50-12-C-on-SU [ERA5]). GEM50-12-C-on-P3 [ERA5] tends to produce more or less precipitation depending on the regime considered (Figure 1.5a). GEM50-12-C-on-P3 [ERA5] produces more precipitation for most environmental conditions compared to GEM50-12-C-on-SU [ERA5] with the exception of regimes with water vapor greater than 30 mm and near-zero vertical pressure velocity (Figure 1.5b). GEM50-12-C-on-P3 [ERA5] shows a higher frequency of precipitation than GEM50-12-C-on-SU [ERA5] (Figure 1.5c), meaning that the simulation using Sundqvist is closer to observations for the frequency of precipitation. Surprisingly, GEM50-12-C-on-P3 [ERA5] and GEM50-12-C-on-SU [ERA5] produces the exact same probabilities for regime with $\omega \leq$ -2.2 Pa s^{-1}. GEM50-12-C-on-P3 [ERA5] shows lower precipitation intensities than GEM50-12-C-on-SU [ERA5] (Figure 1.5d), indicating that the simulation using Sundqvist is also closer to observations for precipitation intensity, except for the most extreme intensities. As found when comparing GEM50-12-C-on-SU [ERA5] and IMERG V7, the comparison between GEM50-12-C-on-P3 [ERA5] and GEM50-12-C-on-SU [ERA5] also shows that a simulation producing precipitation too often generally has a lower intensity of hourly precipitation. The *Annexe B* shows the difference between GEM50-12-C-on-P3 [ERA5] and GEM50-12-C-on-SU [ERA5], relative to the sum of their total precipitation in each regime.

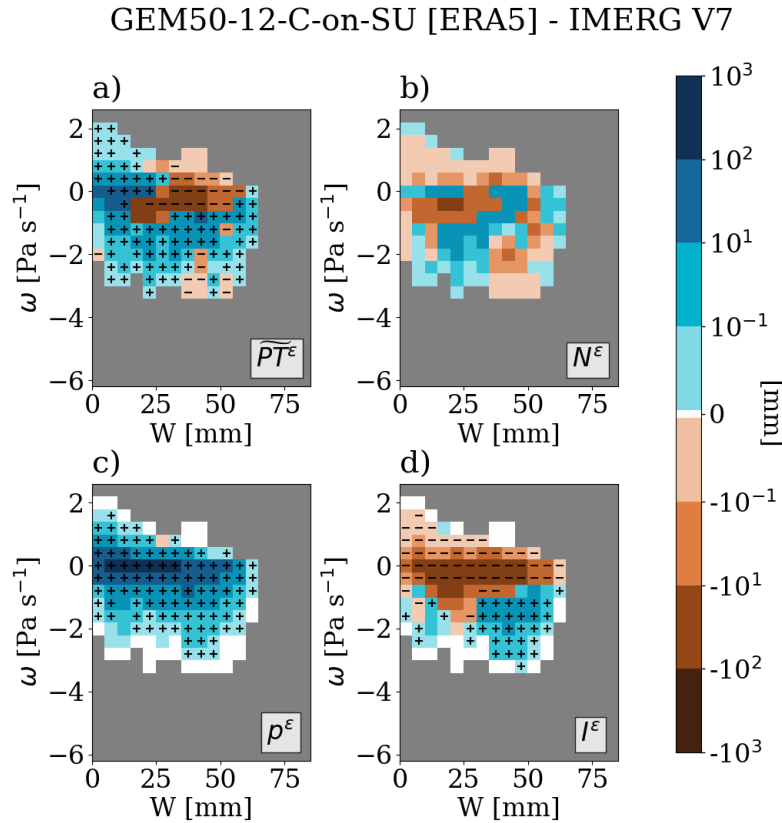GEM50-12-C-on-P3 [ERA5] -
GEM50-12-C-on-SU [ERA5]

Figure 1.5 GEM50-12-C-on-P3 [ERA5] difference against GEM50-12-C-on-SU [ERA5] for the total precipitation per grid point (a) and the three decomposition terms : environment error (b), frequency error (c), and intensity error (d). The white regimes represent errors that are defined as null (see Section1.3.2). Only regimes with at least five precipitating events are considered in this analysis.

1.4.3 GEM5-2.5 precipitation errors decomposition

Figure 1.6 shows the GEM50-2.5-C-on-P3 [ERA5] simulation errors evaluated against the IMERG V7 dataset for all ECIF decomposition error terms. GEM50-2.5-C-on-P3 [ERA5] systematically overestimates total precipitation except for regimes with vertical pressure velocities between 0.2 Pa s^{-1} and -0.6 Pa s^{-1}, where it underestimates the total precipitation (Figure 1.6a). A similar pattern is seen in the environment error term, which shows an overestimation for regimes with vertical velocities $\omega \leq$ -0.6 Pa s^{-1}, and an underestimation for regimes with ω between 0.2 Pa s^{-1} and -0.6 Pa s^{-1} (Figure 1.6b). GEM50-2.5-C-on-P3 [ERA5] shows an underestimation of frequency for regimes with $W \geq$ 25 mm and $\omega \leq$ -0.2 Pa s^{-1} and a higher frequency than observations for regimes associated with smaller value of W (Figure 1.6c). GEM50-2.5-C-on-P3 [ERA5] underestimates the precipitation intensity for positive and slightly negative vertical pressure velocity ($\omega \geq$ -0.6 Pa s^{-1}). For integrated water vapor greater than 30 mm and vertical pressure velocity stronger than

-0.06 Pa s^{-1}, the simulation overestimates intensity (Figure 1.6d). For all error terms, the sign of the bias appears to be robust to the choice of observational product (Figure 1.6a-c-d). Finally, Figure 1.6 shows that GEM50-2.5-C-on-P3 [ERA5] produces much lower values of ω ($\omega \leq$ -3 Pa s^{-1}) than the ERA5 reanalysis, thus overestimating the precipitation in Figure 1.6b. Furthermore, Figure B.3 in the *Annexe B* shows that the environment errors normalized by the sum of the total precipitation play an important role in the total precipitation error.
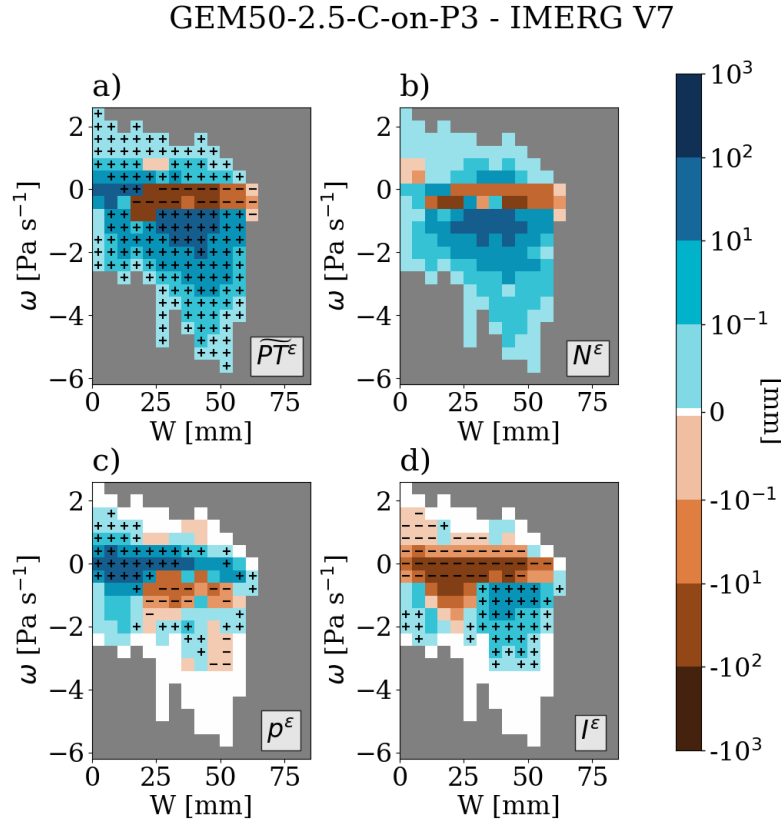
Figure 1.6 GEM50-2.5-C-on-P3 [ERA5] error against IMERG V7 for the total precipitation per grid point (a) and the three decomposition terms : environment error (b), frequency error (c), and intensity error (d). The markers in panels a, c and d indicate the regimes where there is an agreement in the sign of the error using IMERG V6 and Stage IV. The white regimes represent errors that are defined as null (see Section1.3.2). Only regimes with at least five precipitating events are considered in this analysis.

Figure 1.7 shows the difference between the ECIF decomposition terms for the 2.5-km simulation using the P3 microphysics scheme (GEM50-2.5-C-on-P3 [ERA5]) and the one using the Sundqvist condensation scheme (GEM50-2.5-C-on-SU [ERA5]). GEM50-2.5-C-on-P3 produces more precipitation except for regimes with near-zero and slightly negative ω values and low integrated water vapor values ($W \leq$ 20 mm), where it produces less precipitation (Figure 1.7a). When looking at the environmental conditions, GEM50-2.5-C-

on-P3 [ERA5] produces more precipitation than GEM50-2.5-C-on-SU [ERA5] making the simulation with Sunqvist closer to the reference product (Figure 1.7b). GEM50-2.5-C-on-P3 [ERA5] shows a lower probability of precipitating events for most regimes (Figure 1.7c), suggesting that P3 tends to improve the simulation of this term compares with IMERG V7 data. P3 also tends to improve intensity compared to IMERG V7 (Figure 1.7d). For further information on the discrepancies between the two simulations in terms of their difference relative to the sum of their total precipitation, see *Annexe B*.
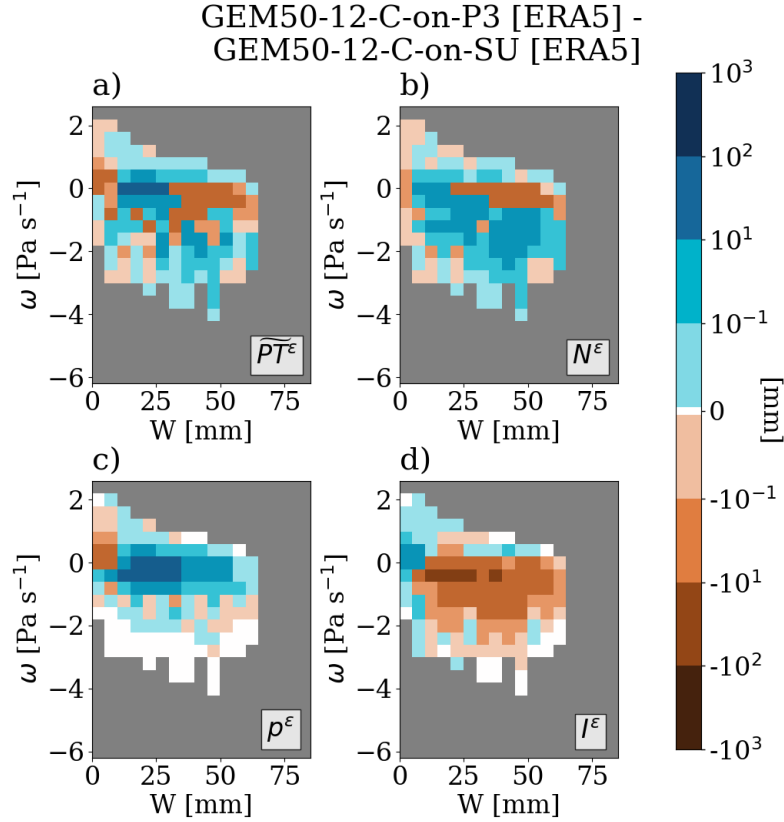

Figure 1.7 GEM50-2.5-C-on-P3 [ERA5] difference against GEM50-2.5-C-on-SU [ERA5] for the total precipitation per grid point (a) and the three decomposition terms : environment error (b), frequency error (c), and intensity error (d). The white regimes represent errors that are defined as null (see Section1.3.2). Only regimes with at least five precipitating events are considered in this analysis.

To evaluate the impact of a multiple nesting approach, we compared GEM50-2.5-C-off-P3 [GEM50-12-SU] with GEM50-2.5-C-off-P3 [ERA5] (Figure 1.8). The total precipitation error per grid point shows that the use of a multiple nesting approach produces less precipitation for regimes with $W \geq 30$ mm while it produces more precipitation for regimes with $W \leq 30$ mm (Figure 1.8a). Using a multiple nesting approach has an impact on the environmental conditions leading to more precipitation for integrated water vapor below 45 mm while less precipitation is observed for regimes with higher values of integrated water vapor 1.8 b).

Figure 1.8 c) shows that GEM50-2.5-C-off-P3 [GEM50-12-SU] tends to produce less precipitation for water vapor values under 45 mm while the opposite occurs when the vertically integrated water vapor is over 45 mm. Figure 1.8 c) shows GEM50-2.5-C-off-P3 [GEM50-12-SU] produces less precipitation for most regimes except for near-zero and slightly negative vertical velocities and water vapor values lower than 35 mm. Figure B.5 in *Annexe B* shows differences between the two simulations, relative to the total amount of precipitation in each regime.

Figure 1.*9* shows the sensitivity of the precipitation simulated by the GEM5-2.5 model when the intermediate 12-km simulation used to drive the model is changed. GEM50-2.5-C-off-P3 [GEM50-12-P3] produces less total precipitation for most regimes compared to its counterpart driven by GEM50-12-SU (Figure 1.9 a). This same pattern of differences across regimes is observed for the environment error term, suggesting that this term dominates total errors (Figure 1.9 b). There is no clear pattern of differences for the frequency and the intensity error terms (Figures 1.9 c,d). The differences between the two simulations, normalized by the sum of their total precipitation in each regime is available in *Annexe B*.

The sensitivity of GEM5-2.5 simulated hourly precipitation to changes in the GEM5 version is assessed by comparing simulations GEM51-2.5-C-off-P3 [GEM51-12-P3] and GEM50-2.5-C-off-P3 [GEM50-12-P3] (Figure 1.10). The upgraded version of GEM5 seems to produce more precipitation for regime with higher values of integrated water vapor while it produces less precipitation for the other regimes (Figure 1.10 a). A similar pattern is observed for the environment error term (Figure 1.10 b) while the frequency and the intensity error terms mostly show a compensatory behavior. GEM51-2.5-C-off-P3 [GEM51-12-P3] generally produces more precipitation due to a higher frequency of hourly events (Figure 1.10 c) and less precipitation due to a lower mean intensity of the events (Figure 1.10 d), particularly for regimes with negative ω values. Figure B.7 in the *Annexe B* shows that the environment errors normalized by the sum of the total precipitation is the main contributor in the total precipitation differences.

To analyze the GEM5-2.5 model's sensitivity to the treatment of deep convection, we compare the GEM50-2.5-C-on-P3 [ERA5] and GEM50-2.5-C-off-P3 [ERA5] simulations (Figure 1.11). Differences in total precipitation between the two simulations are generally small with no clear pattern across regimes (Figure 1.11a). Similarly, GEM50-2.5-C-off-P3 [ERA5] shows no clear pattern across regimes for environmental conditions (Figure 1.11 b). The explicit representation of deep convection produces less precipitation through the probability of precipitation events (Figure 1.11c). GEM50-2.5-C-off-P3 [ERA5] produces more precipitation through
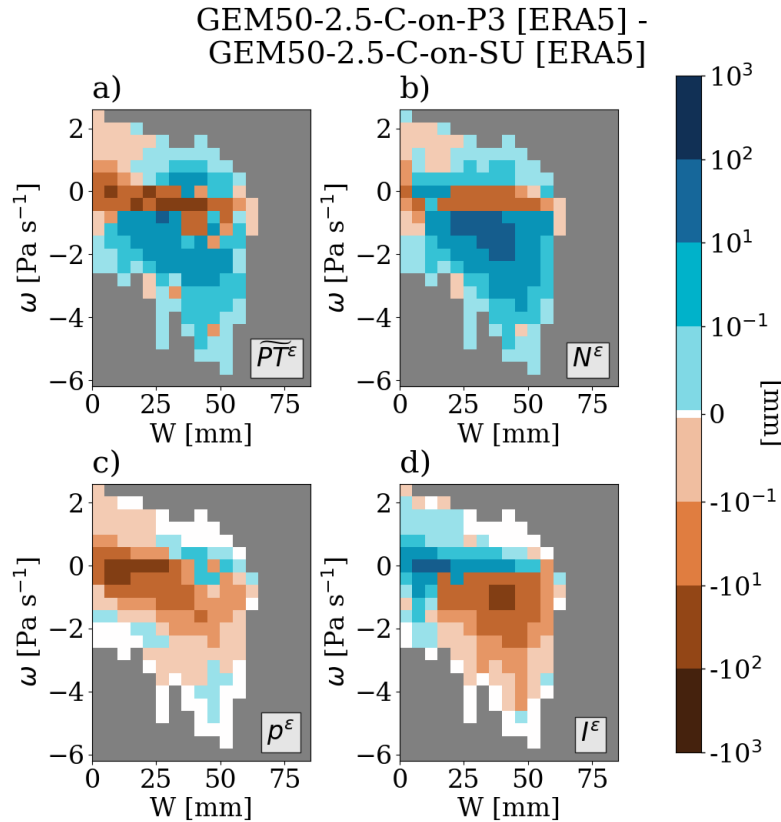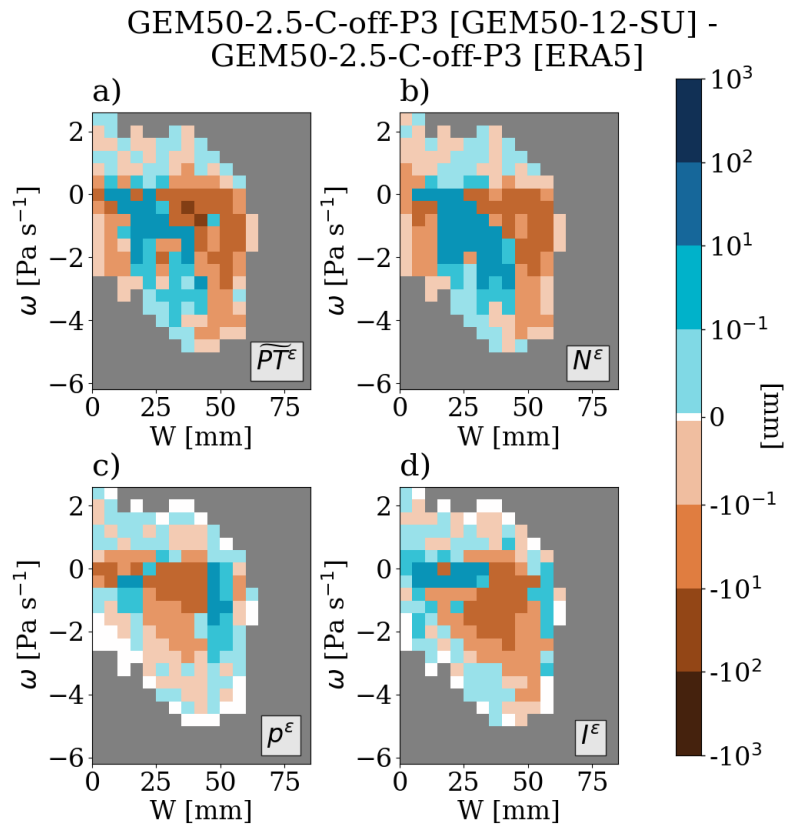
Figure 1.8 GEM50-2.5-C-off [GEM50-12-SU] difference against GEM50-2.5-C-off [ERA5] for the total precipitation per grid point (a) and the three decomposition terms : environment error (b), frequency error (c), and intensity error (d). The white regimes represent errors that are defined as null (see Section1.3.2). Only regimes with at least five precipitating events are considered in this analysis.
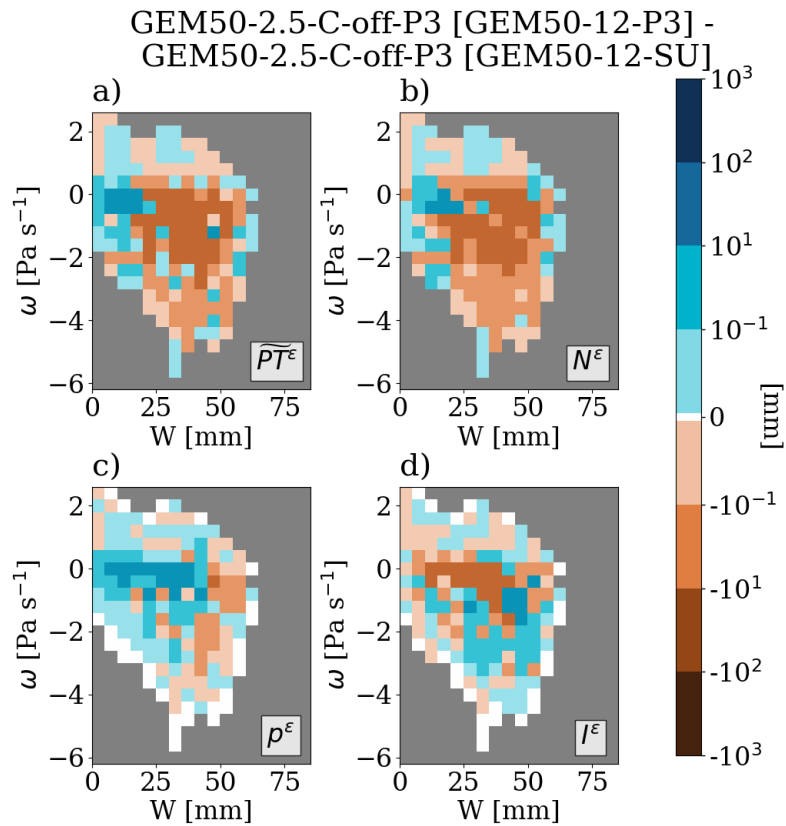
Figure 1.9 GEM50-2.5-C-off [GEM50-12-P3] difference against GEM50-2.5-C-off [GEM50-12-SU] for the total precipitation per grid point (a) and the three decomposition terms : environment error (b), frequency error (c), and intensity error (d). The white regimes represent errors that are defined as null (see Section1.3.2). Only regimes with at least five precipitating events are considered in this analysis.
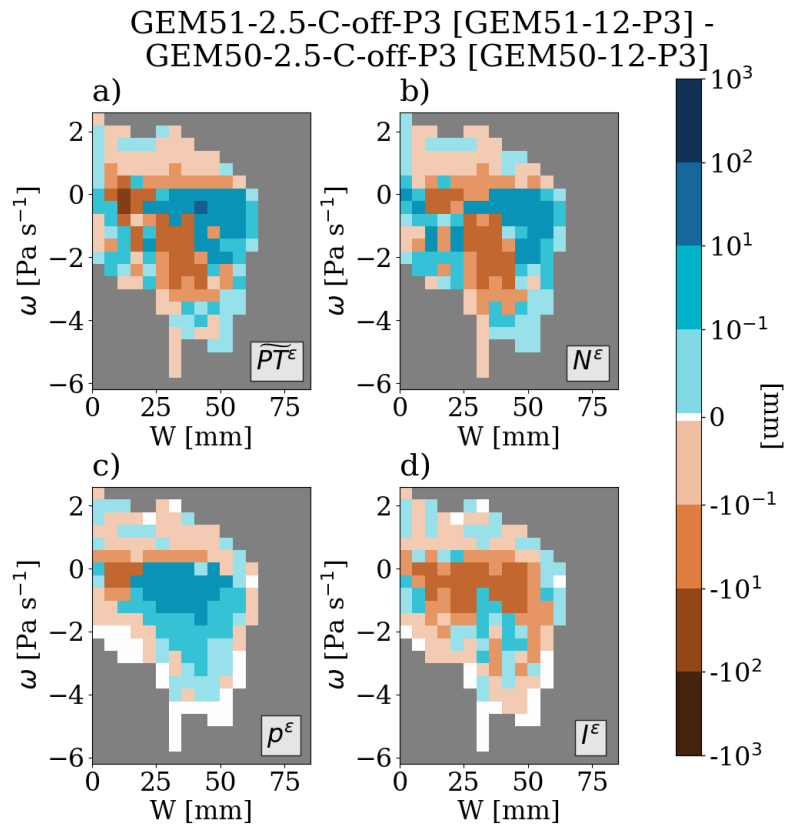
Figure 1.10 GEM51-2.5-C-off [GEM51-12-P3] difference against GEM50-2.5-C-off [GEM50-12-P3] for the total precipitation per grid point (a) and the three decomposition terms : environment error (b), frequency error (c), and intensity error (d). The white regimes represent errors that are defined as null (see Section1.3.2). Only regimes with at least five precipitating events are considered in this analysis.

intensity (Figure 1.11d). Although the differences are small, they are systematic, with a clear compensation between intensity and frequency. The simulation with explicit convection shows less precipitation for frequency terms, which is partially compensated by more precipitation associated with the intensity term. Figure B.8 in the *Annexe B* indicates that the differences between the two simulations are minimal across all error terms. While similar results are obtained by comparing GEM50-2.5-I-off-P3 [ERA5] and GEM50-2.5-I-on-P3 [ERA5] from Figure C.2 in the *Annexe C*.
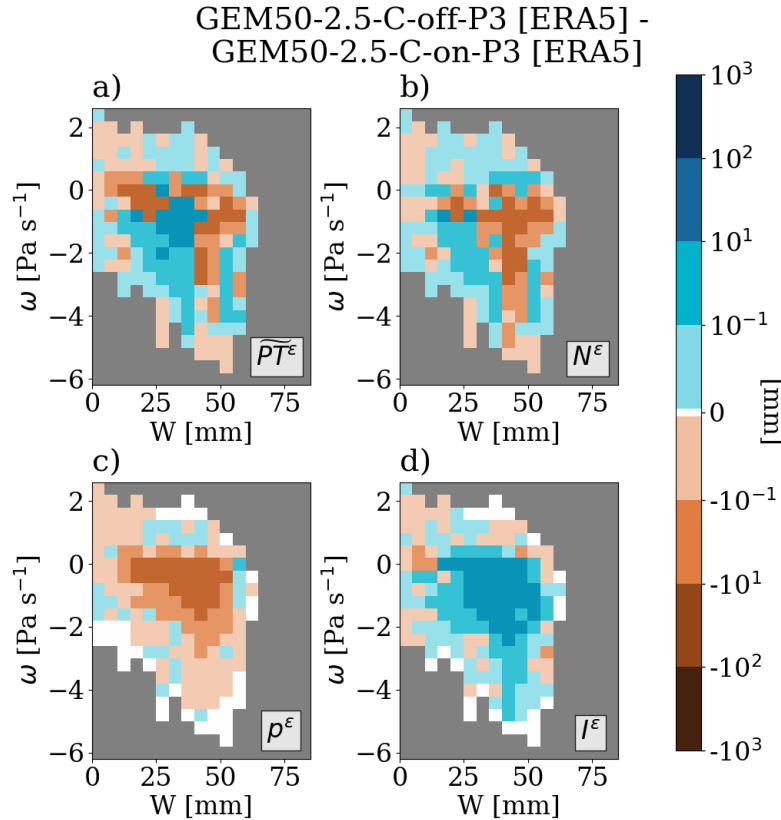
Figure 1.11 GEM50-2.5-C-off-P3 [ERA5] difference against GEM50-2.5-C-on-P3 [ERA5] for the total precipitation per grid point (a) and the three decomposition terms : environment error (b), frequency error (c), and intensity error (d). The white regimes represent errors that are defined as null (see Section1.3.2). Only regimes with at least five precipitating events are considered in this analysis.

The sensitivity of the model to changes in the land surface model was analyzed by comparing GEM50-2.5-I-on-P3 [ERA5] with GEM50-2.5-C-on-P3 [ERA5] (see *Annexe C*, Figure C.1). GEM50-2.5-I-on-P3 [ERA5] generally produces more precipitation through the environment and the intensity, but no clear pattern is defined. In the *Annexe B*, Figure B.9 in the *Annexe B* illustrates that the discrepancies between the two simulations are negligible for all error terms.

1.4.4   Error compensation and the seasonality of sensitivity changes

In this section, two error metrics defined in Equations 1.6 and 1.7 are used to assess all simulations simultaneously. Figure 1.12 depicts the relationship between AAEs (additive absolute errors) and AEs (absolute errors) for individual simulations, observations, and the ERA5 reanalysis, categorized by season. The analysis reveals that AEs range from 0 to approximately 150 mm, while AAEs span from 100 to 1400 mm. The consistently larger AAEs compared to AEs highlight significant compensation effects between different regimes or error terms. Both metrics exhibit their highest values during the summer months (AEs around 150 mm and AAEs approximately 1375 mm). However, this summer peak is strongly dependent on the dataset. It is most evident in the 12-km simulations and ERA5 but less pronounced for the 2.5-km simulations and observations, where other seasons can display comparable or larger errors.

In terms of error sensitivity, AAEs and AEs respond differently to changes in model configurations. For example, during the SON season, the GEM50-2.5-C-off-P3 [GEM50-12-P3] model shows the worst performance when evaluated using AEs. However, when evaluated using AAEs, this model shows significantly better performance compared to the GEM50-12 simulations, demonstrating that different error metrics can lead to different interpretations of model sensitivity. The AAE metric is more effective than the AE metric in distinguishing between observations and simulations. For example, all model AAEs are always larger than the observational uncertainty (AAE calculated using Stage IV or IMERG V6), while this is not the case for the AE metric. This is particularly true for the DJF, as all simulations have AE values below 50 mm, which is within the observational uncertainty set by Stage IV at 60 mm. However, when looking at the AAEs in DJF, all simulations show significantly larger errors compared to Stage IV and IMERG V6. Furthermore, the AAEs are also more effective in discriminating between simulations, especially when looking at simulations with different grid spacings. For both the SON and DJF seasons, AEs fail to discriminate between different grid spacings, while AAEs successfully separate simulations based on their performance, showing that GEM5-2.5 simulations perform significantly better than GEM5-12 simulations. GEM50-2.5-C-on-SU [ERA5] is the only exception, where it has a similar performance to GEM5-12 simulations for DJF. The results also show that, for all seasons, the performance of the ERA5 reanalysis in reproducing hourly precipitation is similar to that of the GEM5-12 simulations. All of these results underscore the importance of using AAEs for a more accurate and informative assessment of model performance, especially in detecting subtle differences that may be missed by AEs.

Figure 1.13 shows the individual components of the AAE error as presented in Equation 1.8 to 1.11 for all

37

products and seasons. We calculated the absolute sum errors of the environmental conditions N_ϵ^{AAE}, the triggering of precipitation p_ϵ^{AAE}, the rain intensity I_ϵ^{AAE} and the residual R (Figure 1.13). For all observational products, the environment errors are zero because large-scale environment conditions are always taken from the ERA5 reanalysis. The observational uncertainty, which is largest in winter, is influenced more or less equally by differences in the frequency and intensity terms. The simulated errors are always larger than the observational uncertainty for all individual error terms, except for the frequency error term in summer, where the GEM5-2.5 p_ϵ^{AAE} are of the same magnitude as the error between observations. All GEM5-2.5 simulations perform significantly better than GEM5-12 simulations in representing precipitation initiation, intensity, and residual for all seasons. However, GEM5-12 simulations often show lower error values for the environmental conditions term, e.g. in the summer months. The reasons for these differences are discussed in the next section.

1.5   Discussion

In evaluating the sensitivity of our model to changes in horizontal resolution, we find that increasing the resolution from 12 km to 2.5 km yields significantly larger improvements than those reported by Di Luca et al. (2021). In particular, our simulations show a reduction in AAE of about 50%, with minimal seasonal dependence. This contrasts with Di Luca et al. (2021), where the 2-km simulations improved performance by about 20% compared to the 8-km and 24-km resolutions of the WRF model over both ocean and land grid points. These differences in the magnitude of improvement can be attributed to several factors, including differences in the models used, the time periods evaluated, and the focus of the analyses. While Di Luca et al. (2021) focused only on strong storm events, our study includes all hourly precipitation events throughout the year.

The comparative analysis of the ECIF errors for GEM5-12 and GEM5-2.5 reveals several important insights. GEM5-12 simulations show lower environmental errors than GEM5-2.5 compared to the ERA5 reanalysis, particularly in summer. We speculate that this is due to GEM5-12 being driven not only at the lateral boundaries but also in the interior of the domain by the ERA5 reanalysis, while GEM5-2.5 relies solely on lateral boundary conditions. This difference likely causes GEM5-12's large-scale patterns to align more closely with ERA5, reducing environmental errors, especially during summer when the inflow forcing across the 2.5-km domain is reduced allowing greater divergence as they propagate inward GEM5-2.5 domain. In winter, the stronger inflow at the lateral boundaries leads to more consistent large-scale patterns between GEM5-12
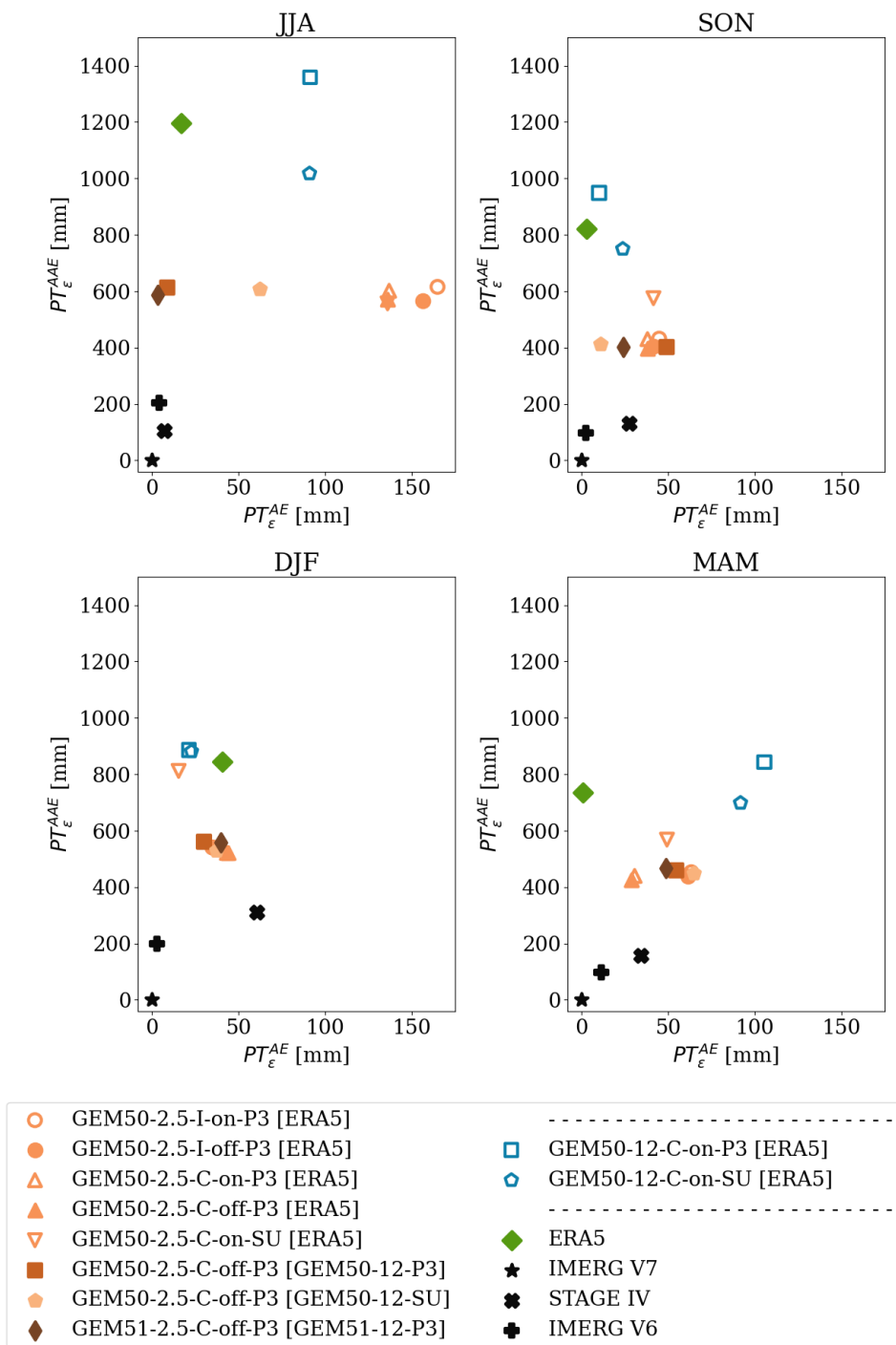
Figure 1.12 Additive absolute errors (AAE) as a function of absolute errors (AE) for all products and for all four seasons. All errors were calculated using the IMERG V7 product as the reference. AAE and AE errors are defined in Section 1.3.2
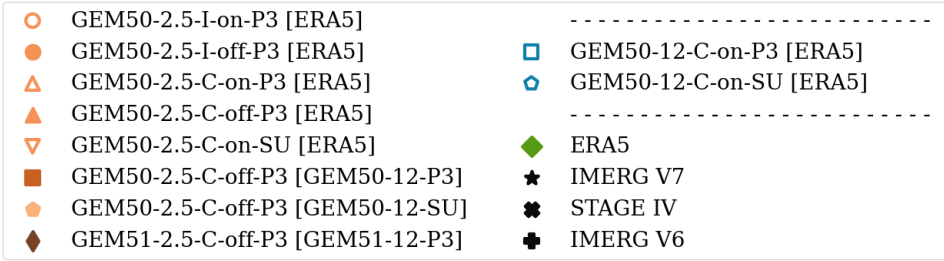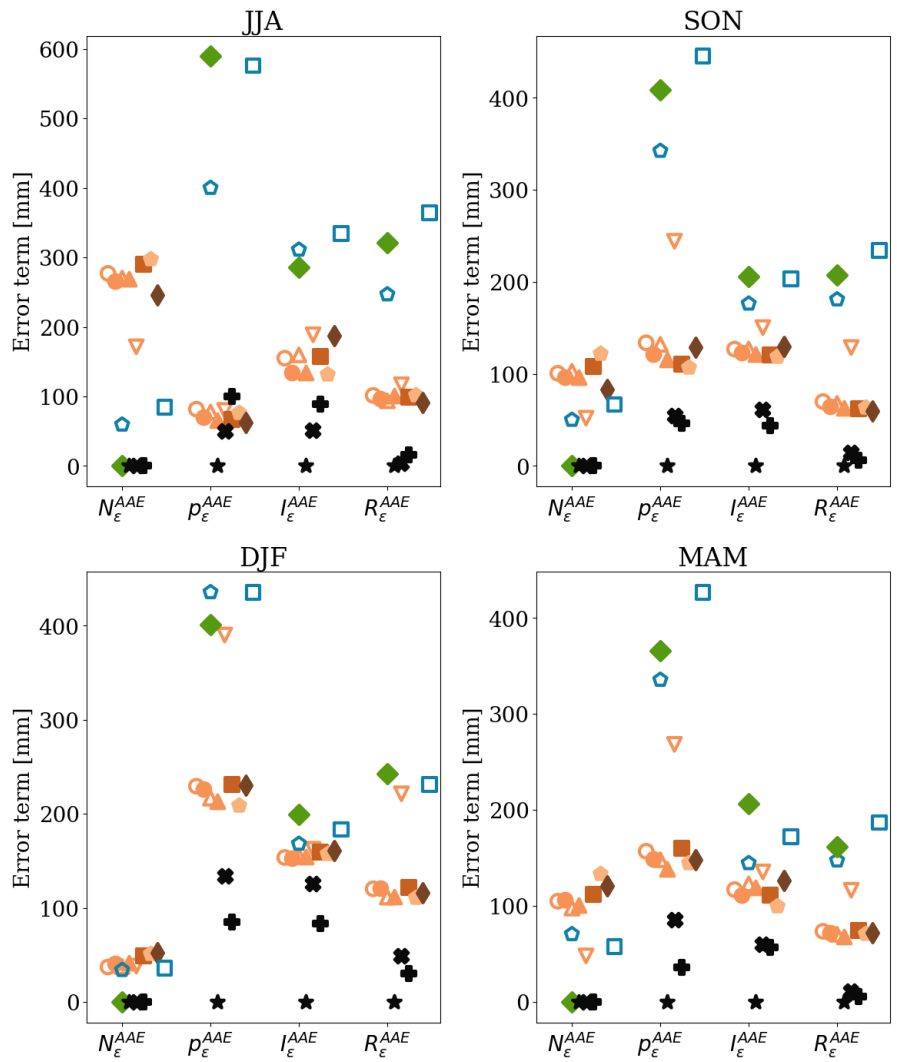
Figure 1.13 Absolute sum errors of environmental conditions N^ϵ, triggering of precipitation p^ϵ, rain intensity I^ϵ and residual R^ϵ for each season. All errors were calculated using the IMERG V7 product as the reference. AAE errors are defined in Section 1.3.2

and GEM5-2.5 simulations, reducing environmental errors in GEM5-2.5 simulations compared to summer (Kalnay et al., 1996; Brankovi and Gregory, 2001; Roberge et al., 2024; Matte et al., 2016; Leduc and Laprise, 2009).

The distribution of error signs across regimes is highly consistent between the two horizontal grid spacings studied, particularly in the total precipitation and intensity terms. Both models exhibit similar intensity error patterns, with precipitation being underestimated under weak dynamical forcing and overestimated under strong dynamical forcing (Figure 1.4d and 1.6d). This behavior is especially pronounced during extreme events, where both GEM5-12 and GEM5-2.5 simulations tend to simulate excessively intense precipitation. Such overestimation of hourly extreme events has also been documented in previous studies. For example, Leutwyler et al. (2017) used a 2.2-km and 12-km version of the COSMO RCM to simulate precipitation over the Alpine region, focusing on hourly precipitation during the 1998-2007 period, and found that the models tended to overestimate the intensity of heavy rainfall events. Even though both GEM5-12 and GEM5-2.5 exhibit consistent error signs for the intensity term, the GEM5-2.5 model adds value during the summer months as shown in Figure 1.13. This finding aligns with Kendon et al. (2012), who conducted a study using a 1.5-km RCM based on the Met Office Unified Model to investigate the realism of hourly rainfall over the United Kingdom. Kendon et al. (2012) found that while the 1.5-km model still tends to slightly overestimate the intensity of these events, it offers a significant improvement over the 12-km version in representing the spatial and temporal characteristics of hourly heavy rain.

The positive bias in precipitation frequency and the negative bias in precipitation intensity in GEM5-12 simulations highlight the model's tendency to trigger too many low-intensity events—known as the 'drizzle bias' (e.g. Sun et al. (2006)). The drizzle bias differs between the two resolutions : while GEM5-12 shows a pronounced drizzle bias for most regimes, GEM5-2.5 only shows a drizzle bias for regimes with low integrated water vapor values. This result aligns with Kendon et al. (2012), as they showed in their study over the United Kingdom that the drizzle bias in the 12-km RCM was considerably reduced in the 1.5-km RCM over land. Stephens et al. (2010) noted in their examination of the performance of three advanced climate and numerical weather prediction models over the oceans that with increased horizontal resolution, models reduce the frequency of light precipitation, but often overcompensate by increasing intensity. Although our results differ slightly over lands, we also observed a see-saw pattern between intensity and frequency.

The frequency and intensity of precipitation is strongly impacted by the representation of processes related

to microphysics and precipitation, with P3 showing even higher frequency of precipitation than Sundqvist. Consequently, simulations performed with the Sundqvist scheme generally perform better, particularly in the summer months. These findings are consistent with some previous studies (Chosson et al., 2014; Jouan et al., 2020). For instance, using version 3 of the GEM model with a 15-km grid spacing,Chosson et al. (2014) showed that incorporating a subgrid cloud and precipitation fraction scheme with a two-moment bulk scheme (similar to P3) led to earlier condensation of water vapor, prolonging cloud longevity, and increasing surface precipitation amounts. They emphasized that the subgrid approach allowed for precipitation to occur before the entire grid box reached saturation, effectively enhancing rainwater production and surface precipitation totals. Jouan et al. (2020), working with the GEM model at a 25 km horizontal resolution, found that the already positive moist precipitation bias in the Sundqvist scheme was exacerbated when the P3 scheme incorporated the subgrid cloud and precipitation fraction system. They hypothesized that the larger quantity of surface precipitation produced by P3 with subgrid fractions was due to a combination of its smaller autoconversion rate compared to Sundqvist and the greater removal of cloud water through accretion by prognostic precipitation. Our results, conducted at a finer resolution of 12 km, further support these insights. Similar to Chosson et al. (2014), we observe that the subgrid cloud and precipitation fraction enhances precipitation efficiency in P3, contributing to higher frequency of precipitation. However, consistent with Jouan et al. (2020), the frequency bias in P3 persists, particularly during summer months. The Sundqvist scheme extended use and tuning in operational large-scale numerical weather prediction models likely contribute to its superior performance in simulating summer precipitation events across resolutions and studies.

Our results show that the impact of using an explicit or parameterized treatment of deep convection on hourly precipitation is minimal. We speculate that this can be attributed to the Kain-Fritsch cumulus scheme being only occasionally triggered in the GEM5-2.5 version of the model. During summer months, the deep convection scheme is triggered between 10% and 30% of precipitation events (D. Paquin-Ricard, personal communication, November 2024). Our results show that the activation of the deep convection scheme increases the frequency of hourly precipitating events while it reduces their intensity across all regimes. Comparing with observations, the increased frequency implies a deterioration by the use of the scheme while it tends to improve the representation of the intensity, especially for regimes with strong precipitation. This behavior may be explained by the Kain-Fritsch scheme's reliance on a trigger parameter that defines the minimum upward velocity (m/s) required to initiate convection, such as cloud formation or precipitation. This mechanism reduces the buildup of Convective Available Potential Energy (CAPE), contributing to the

higher frequency of weaker precipitation events (D. Paquin-Ricard, personal communication, November 2024). Consequently, our results appear to be strongly influenced by the specific model configuration.

In this study, we find that the observational uncertainty is relatively small compared to the model errors, even when considering individual error terms. Given that some of the observations considered are largely independent (e.g., STAGE4 and IMERG), our results suggest that errors are intrinsic to the models, rather than due to observational limitations. For some specific error terms such as the frequency error in summer season, model errors are nearly as small as the observational uncertainty suggesting that the models are approaching the limits of current observational accuracy. In addition, over the domain of interest (northeast North America), the observational uncertainty is largest during winter months. This is in agreement with Picart et al. (2024) in their evaluation of several high-resolution observations over North America. Observational uncertainty peaks in winter in the northern mid-latitudes due to the challenges of satellite retrievals in snow-covered areas (Picart et al., 2024). Without high-quality, high-resolution observations, it's difficult to determine whether models are accurately simulating reality or whether discrepancies are due to observational limitations.

1.6 Summary and Conclusions

This study examined the performance and sensitivity of the CRCM6-GEM5 model in simulating hourly precipitation in northeastern North America. Multiple configurations of the model were considered, including two horizontal grid spacings, two schemes representing subgrid-scale microphysics and precipitation processes, two strategies for the treatment of deep convection, two land surface models, two alternative driving strategies and two model versions. The performance was assessed using independent, state-of-the-art, high-resolution observational datasets in conjunction with a sophisticated multivariate error methodology. This approach incorporates information about the physical processes behind the precipitation field and effectively highlights possible error compensations.

Our results show that the 12-km version of the model overestimates the frequency of precipitation events and underestimates their intensity, especially under weak dynamical forcing. The finer 2.5-km version of the model adds significant value, mainly by improving the hourly precipitation frequency. This is true for all seasons. Our results suggest that the GEM5-2.5 model's hourly precipitation is generally not highly sensitive to variations in subgrid-scale physics, including the activation of a deep convection scheme, the GEM5 model version, the land surface scheme, or the driving strategy. In the 2.5-km version, the largest diffe-

rences appear when replacing the P3 microphysics scheme with the condensation scheme of Sundqvist, and this leads to a much worse performance mainly due to larger errors in the frequency and intensity of hourly precipitation. When using a parameterized approach for deep convection in the GEM5-2.5 model, the differences observed are minimal, with only marginal improvements when using the version with fully explicit convection during the summer. The explicit version shows a lower frequency of hourly events, but with higher intensities. Finally, regarding the driving strategy, our results indicate that using single or double nesting has a relatively minor impact on the hourly precipitation simulated by the 2.5-km model. However, this result should be interpreted with caution, as all intermediate simulations incorporate interior nudging, ensuring a high degree of consistency between the ERA5 reanalysis and the intermediate simulations.

Our findings confirm that evaluating the performance of complex models in representing certain aspects of the climate, such as hourly precipitation, is highly dependent on the error metric used (Di Luca et al., 2021; Whittaker et al., 2024). Furthermore, the results indicate that a coherent understanding of observational uncertainty and simulated errors is achieved only when considering intricate physical interactions (e.g., additive absolute errors) rather than relying on simple metrics like bias or absolute error. While it is important to acknowledge that a model's ability to reproduce past climate conditions does not necessarily ensure accurate simulation of future climates, using evaluation metrics that account for multiple regimes with diverse dynamic and thermodynamic forcings can enhance confidence in climate projections. This method is also well suited to decompose the precipitation response to future changes in the climate, as done in Wallace et al. (2023).

Although the evaluation framework used in this study proved effective in identifying compensatory errors, it focuses on a limited number of variables and on a specific vertical level. For example, recent studies (Wallace et al., 2023) have shown that a significant portion of precipitation occurs in environments characterized by weak to moderate subsidence (positive ω), suggesting that accounting for ω at a single isobaric level may not capture all types of precipitation. Such precipitation, which occurs in regimes with positive ω, can be stratiform in nature or locally forced by orography, independent of the dynamic forcing at 500 hPa (Wallace et al., 2023). It is therefore essential to recognize that this strategy may not account for all triggers of precipitation in our study domain, where precipitation results from multiple phenomena across different scales (e.g., fronts, depressions, deep and shallow convection, etc.) that can interact with one another (e.g. Houze Jr, 2014).

CONCLUSION

Ce mémoire a évalué l'évaluation de la performance et de la sensibilité du Modèle Régional Canadien du Climat (MRCC6-GEM5) dans la simulation des précipitations horaires sur le nord-est de l'Amérique du Nord. Les modèles climatiques, et en particulier les modèles régionaux à haute résolution comme le CRCM6-GEM5, sont des outils essentiels pour simuler les processus complexes du système climatique terrestre. Ces modèles sont cruciaux pour projeter les réponses du climat aux forçages anthropiques et naturels, offrant ainsi des projections futures de changement climatique indispensables à la planification et à l'adaptation aux changements climatiques (Trenberth, 2011; Field et al., 2012).

L'évaluation de la performance des modèles est une étape clé pour renforcer la confiance dans les projections climatiques. Cependant, il est important de reconnaître que la capacité d'un modèle à reproduire le climat actuel et passé ne garantit pas nécessairement qu'il simulera fidèlement le climat futur, surtout lorsque de nouveaux régimes climatiques émergent ou que des interactions non-linéaires se manifestent. C'est ici que réside l'importance de méthodologies robustes, comme la décomposition intensité-fréquence conditionnée par l'environnement employée dans cette étude, qui permettent d'évaluer la performance des modèles selon divers régimes climatiques. Cette méthode permet d'évaluer la performance du modèle selon plusieurs régimes climatiques caractérisés par des forçages dynamiques et thermodynamiques, tout en offrant une meilleure compréhension des sources d'erreurs spécifiques.

Les résultats de cette étude ont montré que les erreurs de précipitation totales peuvent être efficacement décomposées en trois composantes : l'environnement, la fréquence, et l'intensité des événements de précipitation. Cette décomposition a révélé des compensations d'erreurs importantes, notamment dans les simulations effectuées à des résolutions de 12 km, où la fréquence des événements de précipitation est souvent surestimée tandis que leur intensité est sous-estimée. À l'inverse, les simulations à plus haute résolution (2,5 km) ont démontré une valeur ajoutée significative en réduisant ces erreurs de fréquence. C'est le changement de maillages horizontaux qui a eu l'impact le plus significatif sur la représentation des précipitations horaires, car les simulations à 2,5km ont montré une faible sensibilité aux changements de configuration.

Dans ce contexte, l'évaluation du modèle CRCM6-GEM5 à travers la méthode de décomposition ECIF représente une contribution importante à la littérature existante. Cette étude se distingue par son approche

systématique qui compare la performance du modèle à différentes résolutions spatiales, avec divers schémas de microphysique et traitements de la convection. Les résultats obtenus offrent un cadre exhaustif pour évaluer la robustesse du modèle dans la simulation des précipitations horaires. Ce travail fournit des informations essentielles sur la performance du modèle sous des conditions dynamiques et thermodynamiques variées et ouvre la voie à de futures recherches visant à améliorer la précision des modèles climatiques, notamment en ce qui concerne la représentation des événements de précipitation.

L'étude a également mis en lumière l'importance de l'utilisation de plusieurs métriques pour évaluer la performance des modèles. Les erreurs absolues additives se sont avérées plus efficaces que les erreurs absolues simples pour différencier les performances des modèles et pour identifier les divergences entre les simulations et les observations. Cette approche souligne l'importance de considérer les compensations d'erreurs entre variables, un facteur crucial pour affiner la précision des simulations climatiques.

Bien que le cadre d'évaluation utilisé dans cette étude ait prouvé son efficacité dans l'identification des erreurs compensatoires, il se focalise sur un nombre limité de variables et sur un niveau vertical donné. Par exemple, des études récentes (Wallace et al., 2023) ont montré que des quantités non négligeables de précipitations se produisaient dans des environnements caractérisés par une subsidence faible à modérée (ω positif), suggérant que la prise en compte de ω à un seul niveau isobarique pourrait ne pas suffire pour capturer tous les types de précipitation. Ces précipitations, qui se produisent dans des régimes avec ω positif, peuvent être de nature stratiforme ou localement forcées par l'orographie, indépendamment du forçage dynamique à 500 hPa (Wallace et al., 2023). Il est donc essentiel de considérer que cette stratégie pourrait ne pas couvrir tous les déclencheurs de précipitation dans notre domaine d'étude, où les précipitations résultent de multiples phénomènes à différentes échelles (fronts, dépressions, convection profonde et peu profonde, etc.) pouvant interagir entre eux (e.g. Houze Jr, 2014).

En conclusion, ce mémoire souligne l'importance du choix de maillages horizontaux des modèles climatiques régionaux à haute résolution pour améliorer la simulation des précipitations horaires. La méthode ECIF s'est avérée un outil précieux pour décomposer et comprendre les sources d'erreurs dans la modélisation des précipitations.

Cette annexe contient deux figures supplémentaires destinées à compléter l'analyse des produits observationnels utilisés. Elle présente la décomposition des erreurs par la méthode ECIF (Section 1.3.2) entre IMERG V6 et IMERG V7, ainsi qu'entre Stage IV et IMERG V7.
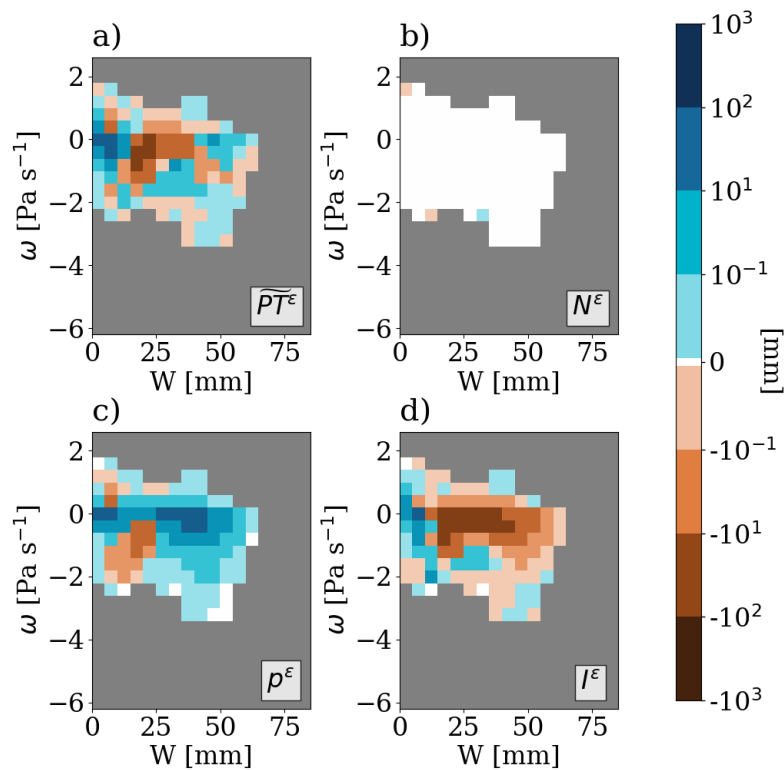
Figure A.1 Différence entre IMERG V6 et IMERG V7 pour la période 2016-2017 pour les précipitations totales par point de grille (a) et les trois termes de décomposition : erreur d'environnement (b), erreur de fréquence (c), et erreur d'intensité (d). Les régimes en blanc représentent des erreurs définies comme nulles (voir section 1.3.2). Seuls les régimes ayant au moins cinq événements de précipitation sont pris en compte dans cette analyse.

Figure A.2 Différence entre Stage IV et IMERG V7 pour la période 2016-2017 pour les précipitations totales par point de grille (a) et les trois termes de décomposition : erreur d'environnement (b), erreur de fréquence (c), et erreur d'intensité (d). Les régimes en blanc représentent des erreurs définies comme nulles (voir section 1.3.2). Seuls les régimes ayant au moins cinq événements de précipitation sont pris en compte dans cette analyse.

ANNEXE B

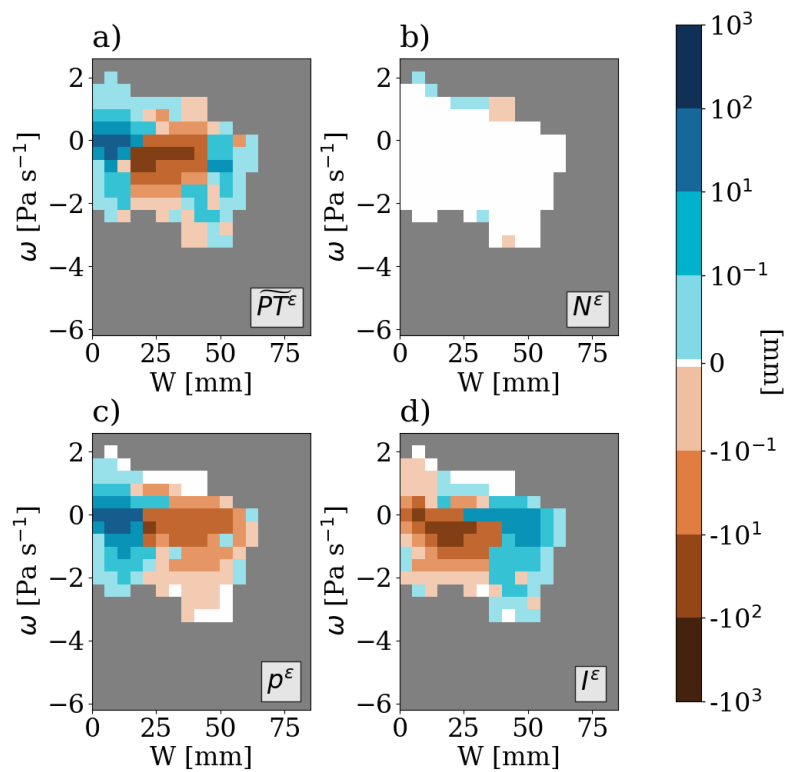## FIGURES SUPPLÉMENTAIRES : ERREURS NORMALISÉES POUR LES SIMULATIONS

Cette annexe contient plusieurs figures supplémentaires destinées à compléter l'analyse de la performance et de la sensibilité. Elle présente les erreurs normalisées issues de la décomposition par la méthode ECIF (Section 1.3.2).

À partir de l'équation 1.4, nous définissons une valeur normalisée par la somme des précipitations totales de l'erreur pour chacun des régimes (i, j) :

$$\widetilde{PT}_n^{\epsilon} = \frac{\widetilde{PT}^{\epsilon}}{(\widetilde{PT}^m + \widetilde{PT}^o)} \tag{B.1}$$

$$N_n^{\epsilon} = \frac{N^{\epsilon}}{(\widetilde{PT}^m + \widetilde{PT}^o)} \tag{B.2}$$

$$p_n^{\epsilon} = \frac{p^{\epsilon}}{(\widetilde{PT}^m + \widetilde{PT}^o)} \tag{B.3}$$

$$I_n^{\epsilon} = \frac{I^{\epsilon}}{(\widetilde{PT}^m + \widetilde{PT}^o)} \tag{B.4}$$

Où $\widetilde{PT}_n^{\epsilon}$, N_n^{ϵ}, p_n^{ϵ} et I_n^{ϵ} sont les erreurs relatives par rapport à la somme des précipitations totales du modèle $(\widetilde{PT}^m)$ et de son produit de comparaison $(\widetilde{PT}^o)$.

Figure B.1 Erreur de GEM50-12-C-on-SU [ERA5] par rapport à IMERG V7, normalisée par la somme de leurs précipitations totales dans chaque régime, pour les précipitations totales par point de grille (a) et les trois termes de décomposition : erreur normalisée de l'environnement (b), erreur normalisée de la fréquence (c), et erreur normalisée de l'intensité (d). Les régimes en blanc représentent des erreurs définies comme nulles (voir Section 1.3.2). Seuls les régimes ayant au moins cinq événements de précipitation sont pris en compte dans cette analyse.

Figure B.2 Différence entre GEM50-12-C-on-P3 [ERA5] et GEM50-12-C-on-SU [ERA5], normalisée par la somme de leurs précipitations totales dans chaque régime, pour les précipitations totales par point de grille (a) et les trois termes de décomposition : erreur normalisée de l'environnement (b), erreur normalisée de la fréquence (c), et erreur normalisée de l'intensité (d). Les régimes en blanc représentent des erreurs définies comme nulles (voir Section 1.3.2). Seuls les régimes ayant au moins cinq événements de précipitation sont pris en compte dans cette analyse.
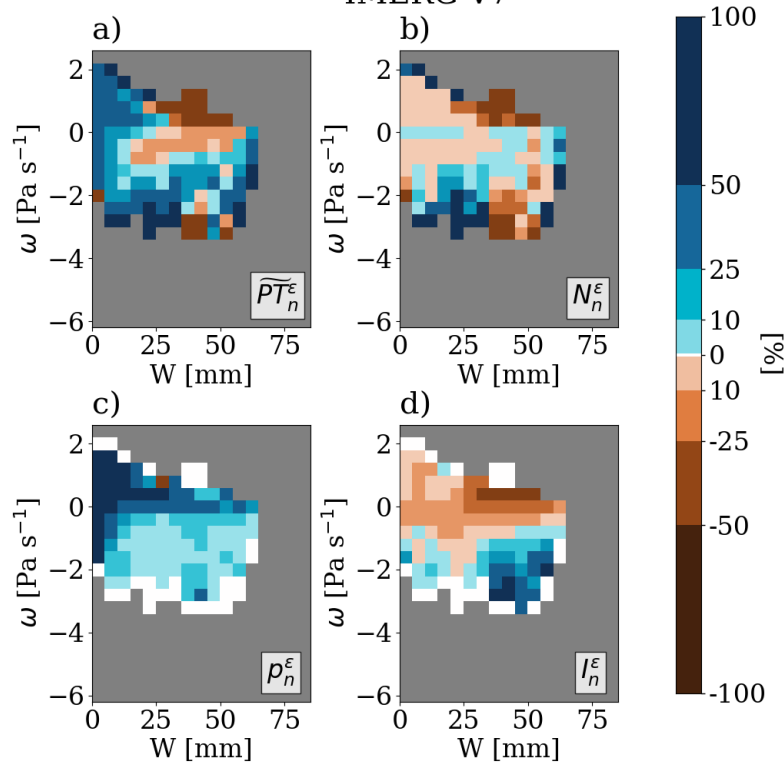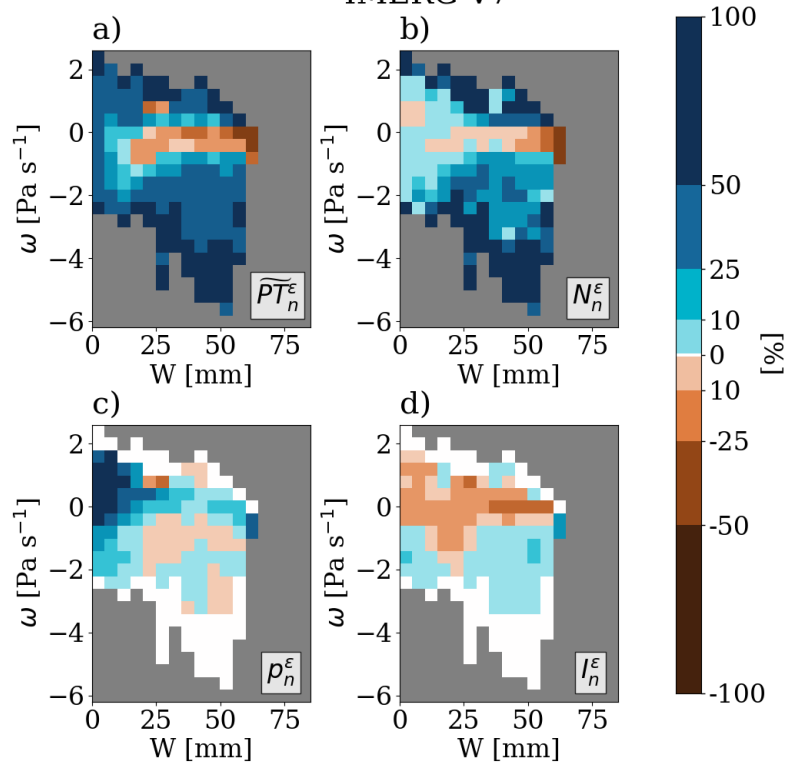
Figure B.3 Erreur de GEM50-2.5-C-on-P3 [ERA5] par rapport à IMERG V7, normalisée par la somme de leurs précipitations totales dans chaque régime, pour les précipitations totales par point de grille (a) et les trois termes de décomposition : erreur normalisée de l'environnement (b), erreur normalisée de la fréquence (c), et erreur normalisée de l'intensité (d). Les régimes en blanc représentent des erreurs définies comme nulles (voir Section 1.3.2). Seuls les régimes ayant au moins cinq événements de précipitation sont pris en compte dans cette analyse.

GEM50-2.5-C-on-P3 [ERA5] -
GEM50-2.5-C-on-SU [ERA5]

Figure B.4 Différence entre GEM50-2.5-C-on-P3 [ERA5] et GEM50-2.5-C-on-SU [ERA5], normalisée par la somme de leurs précipitations totales dans chaque régime, pour les précipitations totales par point de grille (a) et les trois termes de décomposition : erreur normalisée de l'environnement (b), erreur normalisée de la fréquence (c), et erreur normalisée de l'intensité (d). Les régimes en blanc représentent des erreurs définies comme nulles (voir Section 1.3.2). Seuls les régimes ayant au moins cinq événements de précipitation sont pris en compte dans cette analyse.
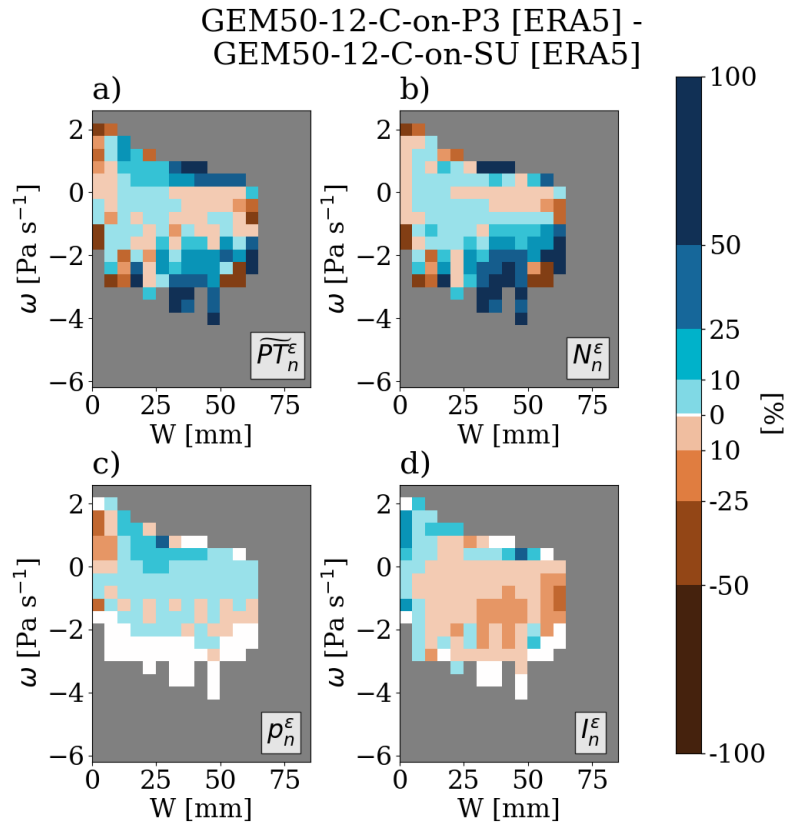
Figure B.5 Différence entre GEM50-2.5-C-off-P3 [GEM50-12-SU] et GEM50-2.5-C-off-P3 [ERA5], normalisée par la somme de leurs précipitations totales dans chaque régime, pour les précipitations totales par point de grille (a) et les trois termes de décomposition : erreur normalisée de l'environnement (b), erreur normalisée de la fréquence (c), et erreur normalisée de l'intensité (d). Les régimes en blanc représentent des erreurs définies comme nulles (voir Section 1.3.2). Seuls les régimes ayant au moins cinq événements de précipitation sont pris en compte dans cette analyse.

GEM50-2.5-C-off-P3 [GEM50-12-P3] -
GEM50-2.5-C-off-P3 [GEM50-12-SU]

Figure B.6 Différence entre GEM50-2.5-C-off-P3 [GEM50-12-P3] et GEM50-2.5-C-off-P3 [GEM50-12-SU], normalisée par la somme de leurs précipitations totales dans chaque régime, pour les précipitations totales par point de grille (a) et les trois termes de décomposition : erreur normalisée de l'environnement (b), erreur normalisée de la fréquence (c), et erreur normalisée de l'intensité (d). Les régimes en blanc représentent des erreurs définies comme nulles (voir Section 1.3.2). Seuls les régimes ayant au moins cinq événements de précipitation sont pris en compte dans cette analyse.
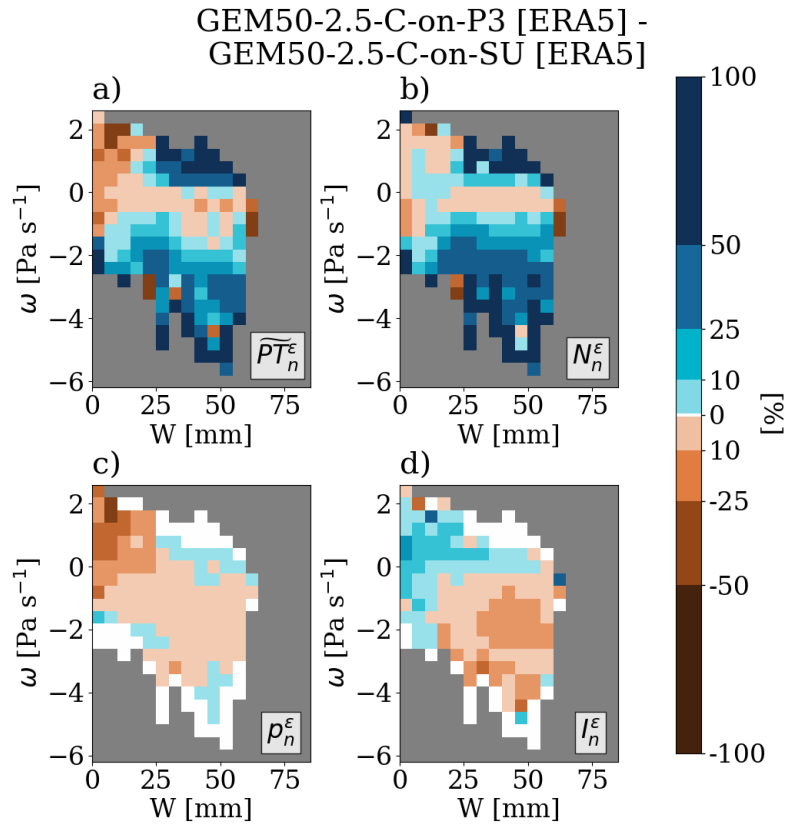
GEM51-2.5-C-off-P3 [GEM51-12-P3] -
GEM50-2.5-C-off-P3 [GEM50-12-P3]
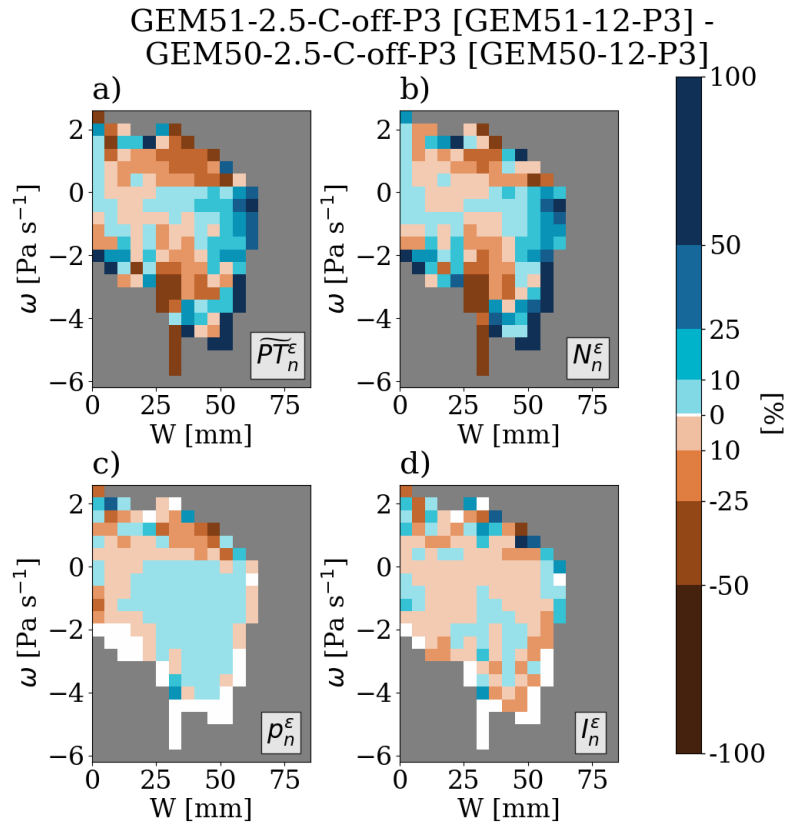
Figure B.7 Différence entre GEM51-2.5-C-off-P3 [GEM51-12-P3] et GEM50-2.5-C-off-P3 [GEM50-12-P3], normalisée par la somme de leurs précipitations totales dans chaque régime, pour les précipitations totales par point de grille (a) et les trois termes de décomposition : erreur normalisée de l'environnement (b), erreur normalisée de la fréquence (c), et erreur normalisée de l'intensité (d). Les régimes en blanc représentent des erreurs définies comme nulles (voir Section 1.3.2). Seuls les régimes ayant au moins cinq événements de précipitation sont pris en compte dans cette analyse.
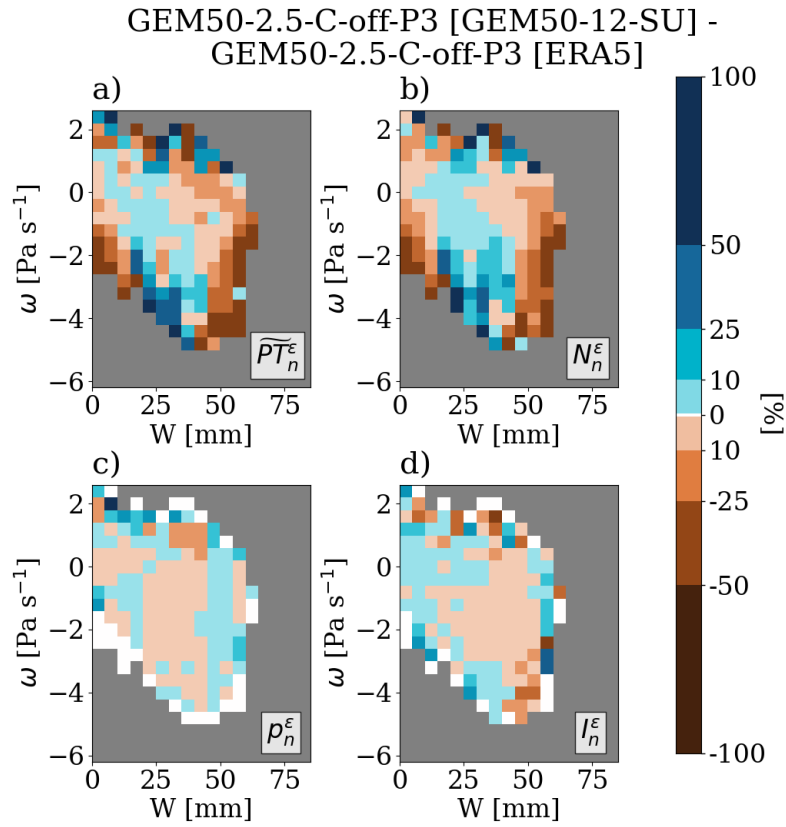
Figure B.8 Différence entre GEM50-2.5-C-off-P3 [ERA5] et GEM50-2.5-C-on-P3 [ERA5], normalisée par la somme de leurs précipitations totales dans chaque régime, pour les précipitations totales par point de grille (a) et les trois termes de décomposition : erreur normalisée de l'environnement (b), erreur normalisée de la fréquence (c), et erreur normalisée de l'intensité (d). Les régimes en blanc représentent des erreurs définies comme nulles (voir Section 1.3.2). Seuls les régimes ayant au moins cinq événements de précipitation sont pris en compte dans cette analyse.
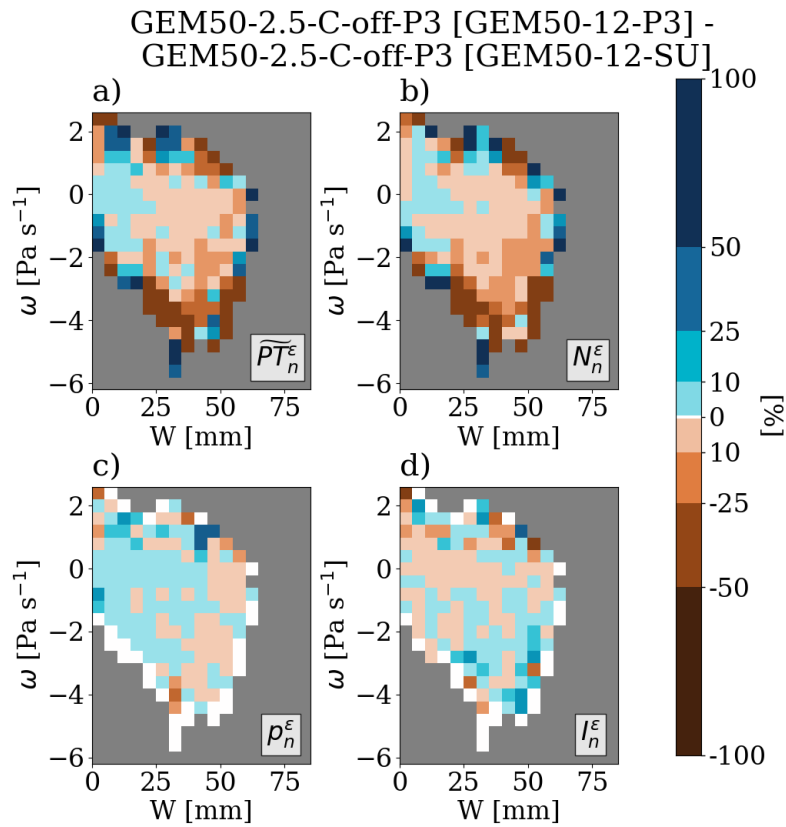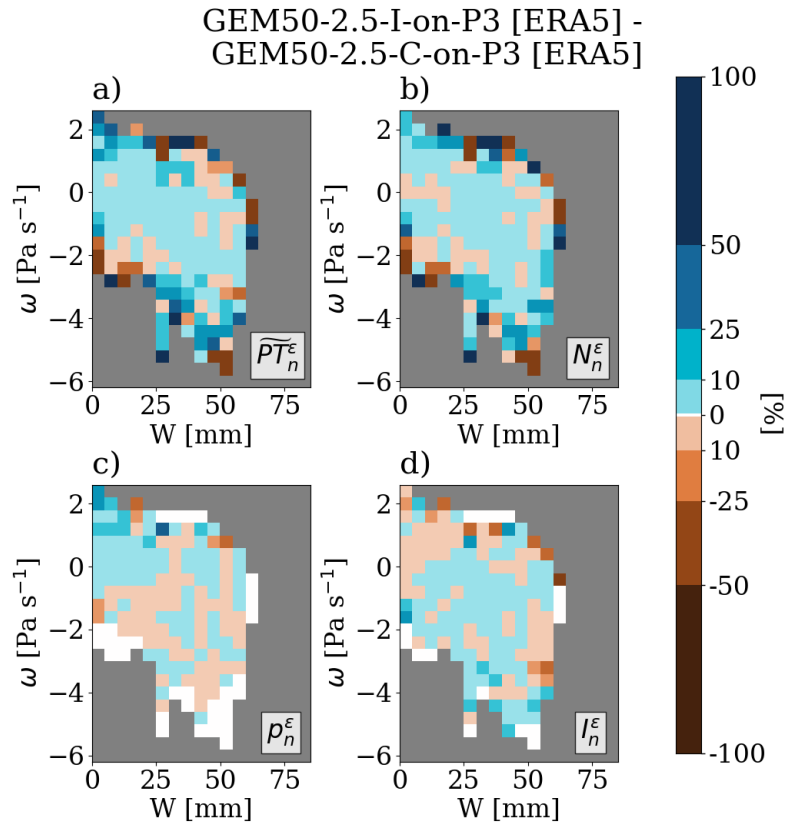
Figure B.9 Différence entre GEM50-2.5-I-on-P3 [ERA5] et GEM50-2.5-C-on-P3 [ERA5], normalisée par la somme de leurs précipitations totales dans chaque régime, pour les précipitations totales par point de grille (a) et les trois termes de décomposition : erreur normalisée de l'environnement (b), erreur normalisée de la fréquence (c), et erreur normalisée de l'intensité (d). Les régimes en blanc représentent des erreurs définies comme nulles (voir Section 1.3.2). Seuls les régimes ayant au moins cinq événements de précipitation sont pris en compte dans cette analyse.

FIGURES SUPPLÉMENTAIRES : DÉCOMPOSITION DES DIFFÉRENCES POUR LES SIMULATIONS

Cette annexe contient deux figures supplémentaires destinées à compléter l'analyse de la sensibilité du modèles MRCC6-GEM5 au schéma de surface (CLASS vs ISBA) et à l'utilisation de la paramétrisation de la convection profonde. Elle présente la décomposition des différences par la méthode ECIF (Section 1.3.2) entre GEM50-2.5-I-on-P3 [ERA5] et GEM50-2.5-C-on-P3 [ERA5], ainsi qu'entre GEM50-2.5-I-off-P3 [ERA5] et GEM50-2.5-I-on-P3 [ERA5].
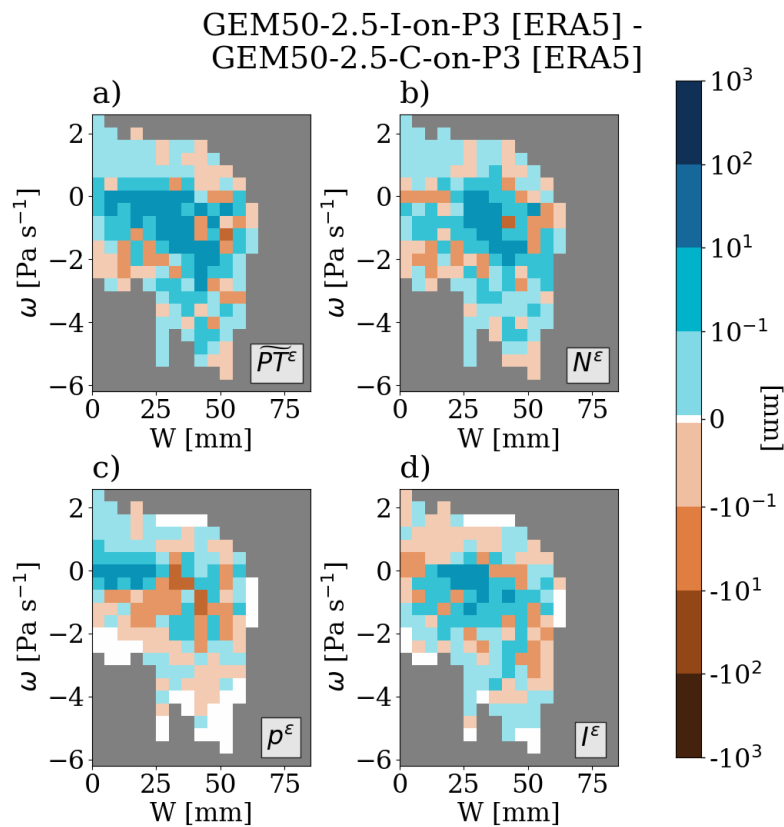
Figure C.1 Différence entre GEM50-2.5-I-on-P3 [ERA5] et GEM50-2.5-C-on-P3 [ERA5] pour la période 2016-2017 pour les précipitations totales par point de grille (a) et les trois termes de décomposition : erreur d'environnement (b), erreur de fréquence (c), et erreur d'intensité (d). Les régimes en blanc représentent des erreurs définies comme nulles (voir section 1.3.2). Seuls les régimes ayant au moins cinq événements de précipitation sont pris en compte dans cette analyse.
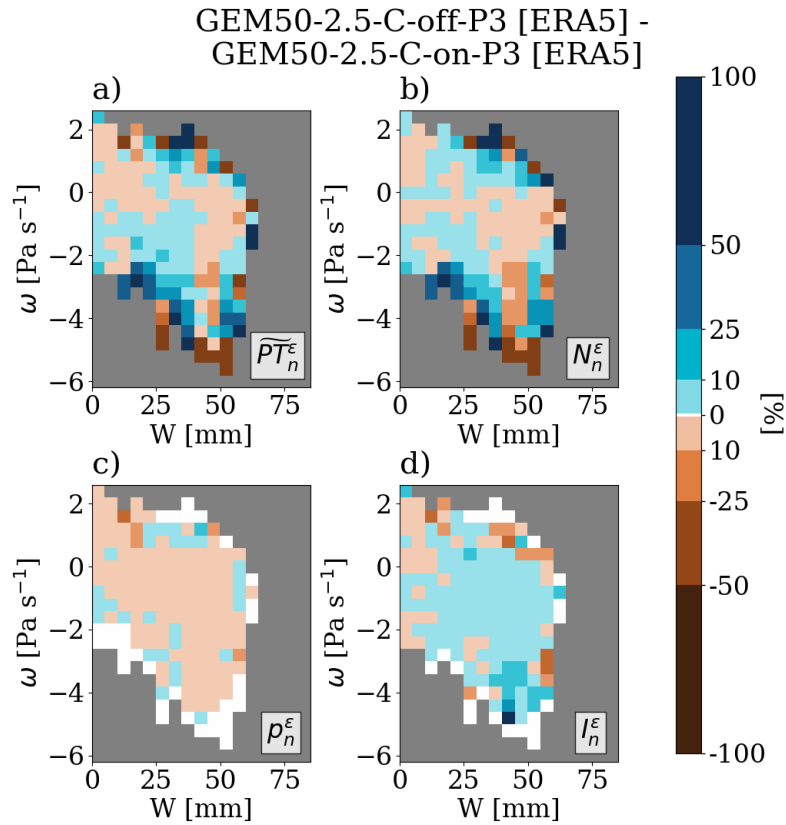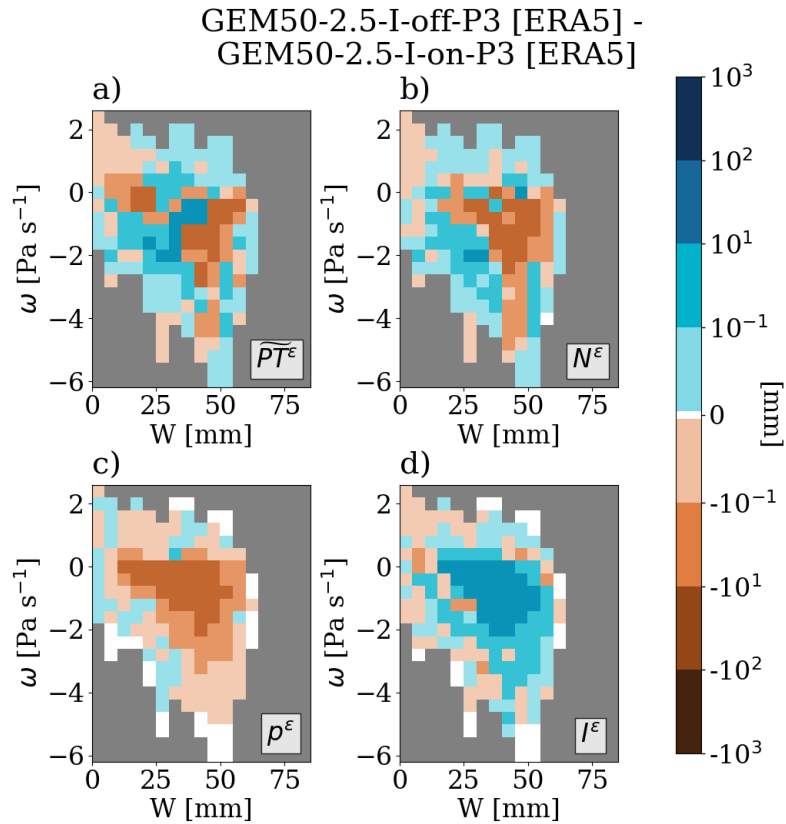
Figure C.2 Différence entre GEM50-2.5-I-off-P3 [ERA5] et GEM50-2.5-I-on-P3 [ERA5] pour la période 2016-2017 pour les précipitations totales par point de grille (a) et les trois termes de décomposition : erreur d'environnement (b), erreur de fréquence (c), et erreur d'intensité (d). Les régimes en blanc représentent des erreurs définies comme nulles (voir section 1.3.2). Seuls les régimes ayant au moins cinq événements de précipitation sont pris en compte dans cette analyse.

BIBLIOGRAPHIE

Arakawa, A. and Jung, J.-H. (2011). Multiscale modeling of the moist-convective atmosphere — A review. *Atmospheric Research*, 102(3) :263–285.

Argüeso, D., Romero, R., and Homar, V. (2020). Precipitation Features of the Maritime Continent in Parameterized and Explicit Convection Models. *Journal of Climate*, 33(6) :2449 – 2466. Place : Boston MA, USA Publisher : American Meteorological Society.

Ban, N., Caillaud, C., Coppola, E., Pichelli, E., Sobolowski, S., Adinolfi, M., Ahrens, B., Alias, A., Anders, I., Bastin, S., Belušić, D., Berthou, S., Brisson, E., Cardoso, R. M., Chan, S. C., Christensen, O. B., Fernández, J., Fita, L., Frisius, T., Gašparac, G., Giorgi, F., Goergen, K., Haugen, J. E., Hodnebrog, , Kartsios, S., Katragkou, E., Kendon, E. J., Keuler, K., Lavin-Gullon, A., Lenderink, G., Leutwyler, D., Lorenz, T., Maraun, D., Mercogliano, P., Milovac, J., Panitz, H.-J., Raffa, M., Remedio, A. R., Schär, C., Soares, P. M. M., Srnec, L., Steensen, B. M., Stocchi, P., Tölle, M. H., Truhetz, H., Vergara-Temprado, J., de Vries, H., Warrach-Sagi, K., Wulfmeyer, V., and Zander, M. J. (2021). The first multi-model ensemble of regional climate simulations at kilometer-scale resolution, part I : evaluation of precipitation. *Climate Dynamics*, 57(1) :275–302.

Ban, N., Schmidli, J., and Schär, C. (2014). Evaluation of the convection-resolving regional climate modeling approach in decade-long simulations. *Journal of Geophysical Research : Atmospheres*, 119(13) :7889–7907.

Bechtold, P., Bazile, E., Guichard, F., Mascart, P., and Richard, E. (2001). A mass-flux convection scheme for regional and global models. *Quarterly Journal of the Royal Meteorological Society*, 127(573) :869–886.

Berthou, S., Kendon, E. J., Chan, S. C., Ban, N., Leutwyler, D., Schär, C., and Fosser, G. (2020). Pan-European climate at convection-permitting scale : a model intercomparison study. *Climate Dynamics*, 55(1) :35–59.

Brankovi, and Gregory, D. (2001). Impact of horizontal resolution on seasonal integrations. *Climate Dynamics*, 18 :123–143.

Bélair, S., Brown, R., Mailhot, J., Bilodeau, B., and Crevier, L.-P. (2003). Operational Implementation of the ISBA Land Surface Scheme in the Canadian Regional Weather Forecast Model. Part II : Cold Season Results. *Journal of Hydrometeorology*, 4(2) :371 – 386. Place : Boston MA, USA Publisher : American Meteorological Society.

Bélair, S., Mailhot, J., Girard, C., and Vaillancourt, P. (2005). Boundary Layer and Shallow Cumulus Clouds in a Medium-Range Forecast of a Large-Scale Weather System. *Monthly Weather Review*, 133(7) :1938 – 1960. Place : Boston MA, USA Publisher : American Meteorological Society.

Chosson, F., Vaillancourt, P. A., Milbrandt, J. A., Yau, M. K., and Zadra, A. (2014). Adapting Two-Moment Microphysics Schemes across Model Resolutions : Subgrid Cloud and Precipitation Fraction and Microphysical Sub–Time Step. *Journal of the Atmospheric Sciences*, 71(7) :2635 – 2653. Place : Boston MA, USA Publisher : American Meteorological Society.

Deng, A. and Stauffer, D. R. (2006). On Improving 4-km Mesoscale Model Simulations. *Journal of Applied Meteorology and Climatology*, 45(3) :361 – 381. Place : Boston MA, USA Publisher : American Meteorological Society.

Di Luca, A., Argüeso, D., Evans, J. P., de Elía, R., and Laprise, R. (2016). Quantifying the overall added value of dynamical downscaling and the contribution from different spatial scales. *Journal of Geophysical Research : Atmospheres*, 121(4) :1575–1590.

Di Luca, A., Argüeso, D., Sherwood, S., and Evans, J. P. (2021). Evaluating Precipitation Errors Using the Environmentally Conditioned Intensity-Frequency Decomposition Method. *Journal of Advances in Modeling Earth Systems*, 13(7) :e2020MS002447.

Di Luca, A., de Elía, R., and Laprise, R. (2015). Challenges in the Quest for Added Value of Regional Climate Dynamical Downscaling. *Current Climate Change Reports*, 1(1) :10–21.

Diaconescu, E. P., Laprise, R., and Sushama, L. (2007). The impact of lateral boundary data errors on the simulated climate of a nested regional climate model. *Climate dynamics*, 28(4) :333–350. Publisher : Springer.

Field, C., Barros, V., Stocker, T., Qin, D., Dokken, D., Ebi, K., Mastrandrea, M., Mach, K., Plattner, G.-K., Allen, S., Tignor, M., and Midgley, P., editors (2012). *Managing the Risks of Extreme Events and Disasters to Advance Climate Change Adaptation (SREX)*. Cambridge University Press, Cambridge, UK.

Findell, K. L. and Eltahir, E. A. B. (2003). Atmospheric Controls on Soil Moisture–Boundary Layer Interactions. Part I : Framework Development. *Journal of Hydrometeorology*, 4(3) :552 – 569. Place : Boston MA, USA Publisher : American Meteorological Society.

Fosser, G., Kendon, E., Chan, S., Lock, A., Roberts, N., and Bush, M. (2020). Optimal configuration and resolution for the first convection-permitting ensemble of climate projections over the United Kingdom. *International Journal of Climatology*, 40(7) :3585–3606.

Fosser, G., Khodayar, S., and Berg, P. (2015). Benefit of convection permitting climate model simulations in the representation of convective precipitation. *Climate Dynamics*, 44(1) :45–60.

Giorgi, F. and Gutowski, W. J. (2015). Regional Dynamical Downscaling and the CORDEX Initiative. *Annual Review of Environment and Resources*, 40(Volume 40, 2015) :467–490. Publisher : Annual Reviews Type : Journal Article.

Hersbach, H., Bell, B., Berrisford, P., Hirahara, S., Horányi, A., Muñoz-Sabater, J., Nicolas, J., Peubey, C., Radu, R., Schepers, D., Simmons, A., Soci, C., Abdalla, S., Abellan, X., Balsamo, G., Bechtold, P., Biavati, G., Bidlot, J., Bonavita, M., De Chiara, G., Dahlgren, P., Dee, D., Diamantakis, M., Dragani, R., Flemming, J., Forbes, R., Fuentes, M., Geer, A., Haimberger, L., Healy, S., Hogan, R. J., Hólm, E., Janisková, M., Keeley, S., Laloyaux, P., Lopez, P., Lupu, C., Radnoti, G., de Rosnay, P., Rozum, I., Vamborg, F., Villaume, S., and Thépaut, J.-N. (2020). The ERA5 global reanalysis. *Quarterly Journal of the Royal Meteorological Society*, 146(730) :1999–2049.

Hohenegger, C., Brockhaus, P., Bretherton, C. S., and Schär, C. (2009). The Soil Moisture–Precipitation Feedback in Simulations with Explicit and Parameterized Convection. *Journal of Climate*, 22(19) :5003 – 5020. Place : Boston MA, USA Publisher : American Meteorological Society.

Houze Jr, R. A. (2014). *Cloud Dynamics*. Academic Press, Amsterdam, 2 edition.

Huffman, G. J., Bolvin, D. T., Braithwaite, D., Hsu, K., Joyce, R., Kidd, C., Nelkin, E. J., Sorooshian, S., Tan, J., and Xie, P. (2018). NASA global precipitation measurement (GPM) integrated multi-satellite retrievals for GPM (IMERG). *Algorithm Theoretical Basis Document (ATBD) Version*, 4.

Huffman, G. J., Bolvin, D. T., Braithwaite, D., Hsu, K.-L., Joyce, R. J., Kidd, C., Nelkin, E. J., Sorooshian, S., Stocker, E. F., Tan, J., Wolff, D. B., and Xie, P. (2020). Integrated Multi-satellite Retrievals for the Global Precipitation Measurement (GPM) Mission (IMERG). In Levizzani, V., Kidd, C., Kirschbaum, D. B., Kummerow, C. D., Nakamura, K., and Turk, F. J., editors, *Satellite Precipitation Measurement : Volume 1*, pages 343–353. Springer International Publishing, Cham.

Huffman, G. J., Bolvin, D. T., Nelkin, E. J., Wolff, D. B., Adler, R. F., Gu, G., Hong, Y., Bowman, K. P., and Stocker, E. F. (2007). The TRMM Multisatellite Precipitation Analysis (TMPA) : Quasi-Global, Multiyear, Combined-Sensor Precipitation Estimates at Fine Scales. *Journal of Hydrometeorology*, 8(1) :38 – 55. Place : Boston MA, USA Publisher : American Meteorological Society.

Jankov, I., Bao, J.-W., Neiman, P. J., Schultz, P. J., Yuan, H., and White, A. B. (2009). Evaluation and Comparison of Microphysical Algorithms in ARW-WRF Model Simulations of Atmospheric River Events Affecting the California Coast. *Journal of Hydrometeorology*, 10(4) :847 – 870. Place : Boston MA, USA Publisher : American Meteorological Society.

Jouan, C., Milbrandt, J. A., Vaillancourt, P. A., Chosson, F., and Morrison, H. (2020). Adaptation of the Predicted Particles Properties (P3) Microphysics Scheme for Large-Scale Numerical Weather Prediction. *Weather and Forecasting*, 35(6) :2541 – 2565. Place : Boston MA, USA Publisher : American Meteorological Society.

Kain, J. S. and Fritsch, J. M. (1990). A One-Dimensional Entraining/Detraining Plume Model and Its Application in Convective Parameterization. *Journal of Atmospheric Sciences*, 47(23) :2784 – 2802. Place : Boston MA, USA Publisher : American Meteorological Society.

Kalnay, E., Kanamitsu, M., Kistler, R., Collins, W., Deaven, D., Gandin, L., Iredell, M., Saha, S., White, G., Woollen, J., Zhu, Y., Chelliah, M., Ebisuzaki, W., Higgins, W., Janowiak, J., Mo, K., Ropelewski, C., Wang, J., Leetmaa, A., Reynolds, R., Jenne, R., and Joseph, D. (1996). The NCEP/NCAR 40-Year Reanalysis Project. *Bulletin of the American Meteorological Society*, 77(3) :437–471.

Kendon, E. J., Roberts, N. M., Senior, C. A., and Roberts, M. J. (2012). Realism of Rainfall in a Very High-Resolution Regional Climate Model. *Journal of Climate*, 25(17) :5791 – 5806. Place : Boston MA, USA Publisher : American Meteorological Society.

Knist, S., Goergen, K., and Simmer, C. (2020). Evaluation and projected changes of precipitation statistics in convection-permitting WRF climate simulations over Central Europe. *Climate Dynamics*, 55(1) :325–341.

Kotlarski, S., Szabó, P., Herrera, S., Räty, O., Keuler, K., Soares, P. M., Cardoso, R. M., Bosshard, T., Pagé, C., Boberg, F., and others (2019). Observational uncertainty and regional climate model evaluation : a pan-European perspective. *International Journal of Climatology*. Publisher : John Wiley & Sons, Ltd.

Leduc, M. and Laprise, R. (2009). Regional climate model sensitivity to domain size. *Climate Dynamics*, 32 :833–854. Publisher : Springer.

Leutwyler, D., Lüthi, D., Ban, N., Fuhrer, O., and Schär, C. (2017). Evaluation of the convection-resolving climate modeling approach on continental scales. *Journal of Geophysical Research : Atmospheres*, 122(10) :5237–5258.

Lin, Y. and Mitchell, K. E. (2005). The NCEP stage II/IV hourly precipitation analyses : Development and applications. In *Proceedings of the 19th Conference Hydrology, American Meteorological Society, San Diego, CA, USA*, volume 10.

Liu, C., Ikeda, K., Thompson, G., Rasmussen, R., and Dudhia, J. (2011). High-Resolution Simulations of Wintertime Precipitation in the Colorado Headwaters Region : Sensitivity to Physics Parameterizations. *Monthly Weather Review*, 139(11) :3533 – 3553. Place : Boston MA, USA Publisher : American Meteorological Society.

Lucas-Picher, P., Argüeso, D., Brisson, E., Tramblay, Y., Berg, P., Lemonsu, A., Kotlarski, S., and Caillaud, C. (2021). Convection-permitting modeling with regional climate models : Latest developments and next steps. *WIREs Climate Change*, 12(6) :e731.

Lucas-Picher, P., Laprise, R., and Winger, K. (2017). Evidence of added value in North American regional climate model hindcast simulations using ever-increasing horizontal resolutions. *Climate Dynamics*, 48(7) :2611–2633.

Mahoney, K., Alexander, M., Scott, J. D., and Barsugli, J. (2013). High-Resolution Downscaled Simulations of Warm-Season Extreme Precipitation Events in the Colorado Front Range under Past and Future Climates. *Journal of Climate*, 26(21) :8671 – 8689. Place : Boston MA, USA Publisher : American Meteorological Society.

Martynov, A., Sushama, L., Laprise, R., Winger, K., and Dugas, B. (2012). Interactive lakes in the Canadian Regional Climate Model, version 5 : the role of lakes in the regional climate of North America. *Tellus A : Dynamic Meteorology and Oceanography*, 64(1) :16226. Publisher : Taylor & Francis.

Matte, D., Laprise, R., and Thériault, J. M. (2016). Comparison between high-resolution climate simulations using single-and double-nesting approaches within the Big-Brother experimental protocol. *Climate Dynamics*, 47 :3613–3626. Publisher : Springer.

McTaggart-Cowan, R., Vaillancourt, P. A., Zadra, A., Chamberland, S., Charron, M., Corvec, S., Milbrandt, J. A., Paquin-Ricard, D., Patoine, A., Roch, M., Separovic, L., and Yang, J. (2019a). Modernization of Atmospheric Physics Parameterization in Canadian NWP. *Journal of Advances in Modeling Earth Systems*, 11(11) :3593–3635.

McTaggart-Cowan, R., Vaillancourt, P. A., Zadra, A., Separovic, L., Corvec, S., and Kirshbaum, D. (2019b). A Lagrangian Perspective on Parameterizing Deep Convection. *Monthly Weather Review*, 147(11) :4127 – 4149. Place : Boston MA, USA Publisher : American Meteorological Society.

Mikyoung Jun, R. K. and Nychka, D. W. (2008). Spatial Analysis to Quantify Numerical Model Bias and Dependence. *Journal of the American Statistical Association*, 103(483) :934–947.

Milbrandt, J. A., Bélair, S., Faucher, M., Vallée, M., Carrera, M. L., and Glazer, A. (2016). The Pan-Canadian High Resolution (2.5 km) Deterministic Prediction System. *Weather and Forecasting*, 31(6) :1791 – 1816. Place : Boston MA, USA Publisher : American Meteorological Society.

Milbrandt, J. A. and Morrison, H. (2016). Parameterization of Cloud Microphysics Based on the Prediction of Bulk Ice Particle Properties. Part III : Introduction of Multiple Free Categories. *Journal of the Atmospheric Sciences*, 73(3) :975 – 995. Place : Boston MA, USA Publisher : American Meteorological Society.

Morrison, H., Milbrandt, J. A., Bryan, G. H., Ikeda, K., Tessendorf, S. A., and Thompson, G. (2015). Parameterization of Cloud Microphysics Based on the Prediction of Bulk Ice Particle Properties. Part II : Case Study Comparisons with Observations and Other Schemes. *Journal of the Atmospheric Sciences*, 72(1) :312 – 339. Place : Boston MA, USA Publisher : American Meteorological Society.

Mote, P., Brekke, L., Duffy, P. B., and Maurer, E. (2011). Guidelines for constructing climate scenarios. *Eos, Transactions American Geophysical Union*, 92(31) :257–258.

Music, B. and Caya, D. (2009). Investigation of the sensitivity of water cycle components simulated by the Canadian Regional Climate Model to the land surface parameterization, the lateral boundary data, and the internal variability. *Journal of Hydrometeorology*, 10(1) :3–21.

Nelson, B. R., Prat, O. P., Seo, D.-J., and Habib, E. (2016). Assessment and Implications of NCEP Stage IV Quantitative Precipitation Estimates for Product Intercomparisons. *Weather and Forecasting*, 31(2) :371 – 394. Place : Boston MA, USA Publisher : American Meteorological Society.

Noilhan, J. and Mahfouf, J.-F. (1996). The ISBA land surface parameterisation scheme. *Global and Planetary Change*, 13(1) :145–159.

Picart, T., Di Luca, A., and Laprise, R. (2024). Uncertainty and outliers in high-resolution gridded precipitation products over eastern North America. *International Journal of Climatology*, 44(4) :1014–1035.

Prat, O. P. and Nelson, B. R. (2015). Evaluation of precipitation estimates over CONUS derived from satellite, radar, and rain gauge data sets at daily to annual scales (2002–2012). *Hydrology and Earth System Sciences*, 19(4) :2037–2056.

Prein, A. F., Holland, G. J., Rasmussen, R. M., Done, J., Ikeda, K., Clark, M. P., and Liu, C. H. (2013). Importance of Regional Climate Model Grid Spacing for the Simulation of Heavy Precipitation in the Colorado Headwaters. *Journal of Climate*, 26(13) :4848 – 4857. Place : Boston MA, USA Publisher : American Meteorological Society.

Prein, A. F., Langhans, W., Fosser, G., Ferrone, A., Ban, N., Goergen, K., Keller, M., Tölle, M., Gutjahr, O., Feser, F., Brisson, E., Kollet, S., Schmidli, J., van Lipzig, N. P. M., and Leung, R. (2015). A review on regional convection-permitting climate modeling : Demonstrations, prospects, and challenges. *Reviews of Geophysics*, 53(2) :323–361.

Pruppacher, H. R. and Klett, J. D. (1997). *Microphysics of Clouds and Precipitation*. Springer, Dordrecht, 2nd edition.

Randall, D., Wood, R., Bony, S., Colman, R., Fichefet, T., Fyfe, J., Kattsov, V., Pitman, A., Shukla, J., Srinivasan, J., Stouffer, R., Sumi, A., and Taylor, K. (2007). Climate Models and Their Evaluation. In Solomon, S., Qin, D., Manning, M., Chen, Z., Marquis, M., Averyt, K., Tignor, M., and Miller, H., editors, *Climate Change 2007 : The Physical Science Basis. Contribution of Working Group I to the Fourth Assessment Report of the Intergovernmental Panel on Climate Change*. Cambridge University Press, Cambridge, United Kingdom and New York, NY, USA.

Roberge, F., Di Luca, A., Laprise, R., Lucas-Picher, P., and Thériault, J. (2024). Spatial spin-up of precipitation in limited-area convection-permitting simulations over North America using the CRCM6/GEM5.0 model. *Geoscientific Model Development*, 17(4) :1497–1510.

Rummukainen, M. (2010). State-of-the-art with regional climate models. *WIREs Climate Change*, 1(1) :82–96.

Schär, C., Lüthi, D., Beyerle, U., and Heise, E. (1999). The Soil–Precipitation Feedback : A Process Study with a Regional Climate Model. *Journal of Climate*, 12(3) :722 – 741. Place : Boston MA, USA Publisher : American Meteorological Society.

Stephens, G. L., L'Ecuyer, T., Forbes, R., Gettelmen, A., Golaz, J.-C., Bodas-Salcedo, A., Suzuki, K., Gabriel, P., and Haynes, J. (2010). Dreary state of precipitation in global models. *Journal of Geophysical Research : Atmospheres*, 115(D24).

Sun, Y., Solomon, S., Dai, A., and Portmann, R. W. (2006). How Often Does It Rain ? *Journal of Climate*, 19(6) :916 – 934. Place : Boston MA, USA Publisher : American Meteorological Society.

Sundqvist, H., Berge, E., and Kristjánsson, J. E. (1989). Condensation and Cloud Parameterization Studies with a Mesoscale Numerical Weather Prediction Model. *Monthly Weather Review*, 117(8) :1641 – 1657. Place : Boston MA, USA Publisher : American Meteorological Society.

Tao, W.-K. and Moncrieff, M. W. (2009). Multiscale cloud system modeling. *Reviews of Geophysics*, 47(4).

Tapiador, F. J., Roca, R., Genio, A. D., Dewitte, B., Petersen, W., and Zhang, F. (2019). Is Precipitation a Good Metric for Model Performance ? *Bulletin of the American Meteorological Society*, 100(2) :223 – 233. Place : Boston MA, USA Publisher : American Meteorological Society.

Tomassini, L. and Yang, G.-Y. (2022). Tropical moist convection as an important driver of Atlantic Hadley circulation variability. *Quarterly Journal of the Royal Meteorological Society*, 148(748) :3287–3302.

Trenberth (2011). Changes in precipitation with climate change. *Climate Research*, 47(1-2) :123–138.

Verseghy, D. L. (1991). Class—A Canadian land surface scheme for GCMS. I. Soil model. *International Journal of Climatology*, 11(2) :111–133.

Wallace, B. C., Haberlie, A. M., Ashley, W. S., Gensini, V. A., and Michaelis, A. C. (2023). Decomposing the Precipitation Response to Climate Change in Convection Allowing Simulations Over the Conterminous United States. *Earth and Space Science*, 10(12) :e2023EA003094.

Whittaker, T., Luca, A. D., Roberge, F., and Winger, K. (2024). Evaluating near-surface wind speeds simulated by the CRCM6-GEM5 model using AmeriFlux data over North America.

Wyngaard, J. C. (2004). Toward Numerical Modeling in the "Terra Incognita". *Journal of the Atmospheric Sciences*, 61(14) :1816 – 1826. Place : Boston MA, USA Publisher : American Meteorological Society.

Zheng, Y., Alapaty, K., Herwehe, J. A., Genio, A. D. D., and Niyogi, D. (2016). Improving High-Resolution Weather Forecasts Using the Weather Research and Forecasting (WRF) Model with an Updated Kain–Fritsch Scheme. *Monthly Weather Review*, 144(3) :833 – 860. Place : Boston MA, USA Publisher : American Meteorological Society.